Table 1. (Continued)

Accession	Probe set ID	Gene name	VO	PO	Molecular function	Reference
Y00497	Y00497_s_at	Superoxide dismutase 2	0.41	0.84	copper, zinc superoxide dismutase activity	
AI229620	rc_AI229620_s_at	Cytochrome c oxidase subunit Vb	0.46	0.95	cytochrome-c oxidase activity, oxidoreductase activity	
X15030	X15030_at	CoxVa for mitochondrial cytochrome c oxidase subunit Va	0.48	0.97	cytochrome-c oxidase activity, oxidoreductase activity	
U95001	U95001UTR#1_s_at	Developmentally-regulated cardiac factor (DRCF-5)	0.44	0.88	diphosphoinositol-polyphosphate diphosphatase activity	
K00750	K00750exon#2-3_g_at	Cytochrome c gene, nuclear gene for mitochondrial product	0.47	0.88	electron transporter activity, lipid binding	
AI176422	rc_AI176422_g_at	Electron-transferring–flavoprotein dehydrogenase	0.47	0.90	electron-transferring–flavoprotein dehydrogenase activity	
M83680	M83680_at	Sprague-Dawley (clone LRB13) RAB14 or GTPase Rab14	0.44	1.02	GTP binding, protein transporter activity	
AA799474	rc_AA799474_at	Similar to cytochrome c-1 (LOC300047)	0.37	0.93	heme binding, electron transporter	
D13120	D13120_s_at	ATP synthase subunit d	0.44	0.81	hydrogen ion transporter activity	*22*
AA875444	rc_AA875444_at	Dihydropyrimidinase-like 2 (Dpysl2)	0.33	0.85	hydrolase activity	
AI235358	rc_AI235358_at	Ubiquinol-cytochrome c reductase core protein II	0.43	0.89	metalloendopeptidase activity	
M20131	M20131cds_s_at	cytochrome P450, family 2, subfamily e, polypeptide 1	0.48	1.16	monooxygenase activity, oxidoreductase activity	
AI013297	rc_AI013297_g_at	NADH dehydrogenase (ubiquinone) Fe-S protein 4	0.47	0.83	NADH dehydrogenase (ubiquinone) activity	
AA819547	rc_AA819547_at	NADH dehydrogenase (ubiquinone) 1α subcomplex	0.47	0.85	NADH dehydrogenase (ubiquinone) activity	
AA851403	rc_AA851403_at	NADH dehydrogenase (ubiquinone) 1β subcomplex 8	0.49	1.04	NADH dehydrogenase (ubiquinone) activity	
AA891651	rc_AA891651_g_at	NADH dehydrogenase (ubiquinone) 1, α/β subcomplex, 1	0.45	0.83	NADH dehydrogenase (ubiquinone) activity, acyl carrier activity	
AF095927	AF095927_g_at	Protein phosphatase 2C	0.48	0.89	negative regulation of cell cycle	
D12769	D12769_g_at	Basic transcription element binding protein 1	0.38	0.91	nucleic acid binding, DNA binding, zinc ion binding	
AA875327	rc_AA875327_g_at	Eukaryotic translation initiation factor 4H	0.44	0.81	nucleotide binding, translation initiation factor activity	
AI136977	rc_AI136977_at	FK506 binding protein 4	0.37	0.87	peptidyl-prolyl *cis-trans* isomerase activity	
U90261	U90261UTR#1_at	Hypertension-regulated vascular factor-1 (HRVF-1)	0.45	0.99	protein binding	
D32209	D32209_at	LANP for leucine-rich acidic nuclear protein	0.48	0.94	protein binding	
AA892544	rc_AA892544_s_at	Neural precursor cell expressed, developmentally down-regulated gene 8	0.49	0.95	protein binding	
AI103838	rc_AI103838_g_at	Heat shock 20-kDa protein (Loc192245)	0.45	0.99	regulation of muscle contraction	
AF090867	AF090867_at	Guanosine monophosphate reductase (GMP-reductase)	0.31	1.12	response to cold	
D84480	D84480_s_at	PMSG-induced ovarian mRNA, 3′ sequence, N2	0.35	0.84	RNA binding, structural constituent of ribosome	
AA900476	rc_AA900476_g_at	Transcription factor MRG1	0.44	0.96	transcription factor activity, transcription cofactor activity	
AA892554	rc_AA892554_g_at	AA891476BAC clone RP24-216M6 from 5	0.49	0.82	—	
D16554	D16554_at	Polyubiquitin (four repetitive ubiquitins in tandem)	0.49	0.92	—	
AA891476	rc_AA891476_at	Similarity to protein pdb:1LBG (E. coli) B Chain B	0.48	0.91	—	
AA946040	rc_AA946040_at	Similar to Uroplakin Ia (UPIa) (UPKa) (LOC365227)	0.49	0.79	—	
AI177256	rc_AI177256_at	EST220870 (ovary derived cDNA)	0.49	0.95	—	
AI011556	rc_AI011556_s_at	EST206007 (ovary derived cDNA)	0.48	1.05	—	
AI010292	rc_AI010292_s_at	EST204743 (Similar to mitochondrial cytochrome oxidase subunit II)	0.44	0.89	—	

Table 1. (Continued)

Accession	Probe set ID	Gene name	VO	PO	Molecular function	Reference
VO↓ and PO↓						
J03481	J03481mRNA_g_at	Dihydropteridine reductase	0.49	0.49	6,7-dihydropteridine reductase activity, oxidoreductase activity	
J02791	J02791_at	Acetyl coenzyme A dehydrogenase medium chain	0.47	0.42	acyl-CoA dehydrogenase activity, oxidoreductase activity	
D00688	D00688_s_at	Monoamine oxidase	0.44	0.43	amine oxidase activity, oxidoreductase activity	
L19998	L19998_at	Minoxidil sulfotransferase	0.49	0.47	aryl sulfotransferase activity, sulfotransferase activity	
AA946532	rc_AA946532_at	Similar to ATP-binding cassette, sub-family D (ALD)	0.27	0.38	ATP binding, ATPase activity	
D49785	D49785_at	Protein kinase (MUK) norvegicus mitogen activated protein kinase	0.33	0.21	ATP binding, cAMP-dependent protein kinase activity	
AI007820	rc_AI007820_s_at	Heat shock 90 kDa protein 1, β	0.48	0.49	ATP binding, nitric-oxide synthase regulator activity	
AI176546	rc_AI176546_at	Heat shock protein 86	0.44	0.49	ATP binding, unfolded protein binding	
AA858640	rc_AA858640_s_at	Heat shock protein 1	0.46	0.46	ATP binding, unfolded protein binding	
AI235707	rc_AI235707_g_at	Calnexin	0.48	0.48	calcium ion binding, sugar binding, unfolded protein binding	
M26125	M26125_at	Epoxide hydrolase 1	0.48	0.47	catalytic activity, aminopeptidase activity	*19*
X60328	X60328_at	Cytosolic epoxide hydrolase	0.36	0.38	catalytic activity, epoxide hydrolase activity, hydrolase activity	
AA818226	rc_AA818226_s_at	Mitochondrial cytochrome c oxidase subunit	0.45	0.49	cytochrome-c oxidase activity, oxidoreductase activity	
AI136891	rc_AI136891_at	Zinc finger protein 36	0.45	0.45	DNA binding, nucleic acid binding	
AI171355	rc_AI171355_s_at	cytochrome b, mitochondrial	0.38	0.46	electron transporter activity	*19*
AA945054	rc_AA945054_s_at	Cytochrome b5	0.39	0.41	electron transporter activity	*19*
AI103396	rc_AI103396_g_at	Mitochondrial gene for cytochrome b	0.49	0.49	electron transporter activity	*19*
AI234604	rc_AI234604_s_at	Heat shock cognate 71 kDa protein	0.46	0.49	heat shock protein activity	
AA818858	rc_AA818858_s_at	Peptidylprolyl isomerase A (Ppia)	0.47	0.47	isomerase activity, peptidyl-prolyl *cis-trans* isomerase activity	
AI228674	rc_AI228674_s_at	Peptidyl-prolyl *cis-trans* isomerase A (PPIase)	0.49	0.49	isomerase activity, peptidyl-prolyl *cis-trans* isomerase activity	
AI103874	rc_AI103874_at	FK506 binding protein 3	0.45	0.49	peptidyl-prolyl *cis-trans* isomerase activity, receptor activity	
AI230406	rc_AI230406_at	RAB10, member RAS oncogene family	0.42	0.45	protein binding, GTP binding, protein transporter activity	
AI007614	rc_AI007614_at	Mitogen-activated protein kinase kinase kinase kinase 4	0.43	0.36	protein kinase activity, small GTPase regulator activity	
AB016532	AB016532_at	rPER2, period homolog 2 (Per2)	0.41	0.44	signal transducer activity	*19*
X62951	X62951mRNA_s_at	Endogenous retrovirus	0.41	0.37	—	
AB013454	AB013454_at	Similar to Ac2-210	0.34	0.32	—	
AI009132	rc_AI009132_at	Similar to chromosome 13 open reading frame 12	0.47	0.47	—	
AA892056	rc_AA892056_at	Similar to deoxycytidyl transferase	0.43	0.46	—	
AI104035	rc_AI104035_s_at	EST213324 (heart derived cDNA)	0.43	0.47	—	
AA945152	rc_AA945152_s_at	EST20065 (liver derived cDNA)	0.32	0.49	—	
AI009141	rc_AI009141_at	EST203592 (embryo derived cDNA)	0.37	0.42	—	

GeneBank accession numbers, probe set ID, gene name, and their functions are listed for each gene. The hold change in gene expression in PO and VO *vs.* sham samples is given. "Reference" indicates that the results were similar to the indicated references.

(LOXL) TaqMan Probe, AGGCAGCCTCCCCCAAGA AGCA; LOXL sense-primer, TTGAAAAGCAGGACCTGC TTC; LOXL antisense-primer, CTCCGGCTAGGCGGCT; pyruvate dehydrogenase kinases-1 (PDK-1) TaqMan Probe, CCGTCGCCACTCTCCATGAAGCA; PDK-1 sense-primer, GGACTTCTATGCGCGCTTCT; PDK-1 antisense-primer, ACTGACCCGAAGTCCAGGAA; transgelin TaqMan Probe, CCGCCCTCCATGGTCTTCAAGCA; transgelin sense-primer, GCCAGTGAAGGTGCCTGAGA; transgelin antisense-primer, AGAATTGAGCCACCTGTTCCA.

Subcloning of Rat MT

Rat MT cDNA was cloned from rat heart by RT-PCR. The following primers were used for this experiment: sense primer, 5′-ACTGCCTTCTTGTCGCTTAC-3′; antisense primer, 5′-AGGGCAGCAGCACTGTTCGT-3′. This PCR product was subcloned into pCR2.1 and then transferred to pcDNA 3.1 (Invitrogen).

Cell Culture and Transfection

H9c2 cells (a cardiac myoblast cell line) were obtained from the American Type Culture Collection (Rockville, USA). Cells were transfected with rat MT-pcDNA3.1 or pcDNA 3.1 (empty vector) by Lipofectamine 2000 (Amersham Biosciences, Piscataway, USA). At 24 h after the transfection, cells were exposed to norepinephrine (NE; 10^{-4} mol/l) and cultured for an additional 24 h. The efficiency of the transfection was assessed by the co-transfection of pQBI50, which encodes blue fluorescent protein (Takara, Tokyo, Japan).

Assessment of Apoptosis and Caspase 3 Assay

Apoptosis was assessed by TUNEL staining (*In Situ* Cell Death Detection kit, Roche Diagnostics, Mannheim, Germany). Caspase-3 activity was measured by a CaspACE assay system (Promega, Madison, USA).

Statistical Analysis

Data are presented as the mean±SEM. Comparisons of mean values were performed by one-way ANOVA followed by Scheffe's test. Values of $p<0.05$ were considered to indicate statistically significant differences.

Results

Figure 1 shows the echocardiographic findings 4 weeks after the surgery. Left ventricular diastolic diameter (LVDd) was significantly higher in the rats subjected to VO compared with those subjected to PO and those undergoing sham operation (hereafter the VO, PO, and sham groups, respectively) (PO: 96±8% of the sham-group value; VO: 119±9% of the sham-group value). While interventricular septal wall thickness (IVST) was increased in both types of hypertrophy (PO, 126±12% of the sham-group value; VO, 120±11% of the sham-group value), the IVST of the PO group was greater than that of the VO group. Thus, PO produced concentric hypertrophy and VO produced eccentric hypertrophy. There was no difference among the PO, VO and sham groups in percent fractional shortening (%FS). The left atrial diameter (LAD) of both hypertrophy groups was larger than that of the sham group. As shown in Fig. 2, the left ventricular weight/body weight ratio and heart weight/body weight ratio were significantly increased in both hypertrophy groups, compared with the sham group. These ratios were slightly larger in the VO than the PO group (PO: 139±11% of the sham-group value; VO: 157±16% of the sham-group value).

Figure 3 and Table 1 show results of DNA chip analysis. A total of 33 genes were upregulated in both forms of hypertrophy, whereas 31 were downregulated. The genes that were upregulated in both forms included BNP, atrial natriuretic peptide (ANP), and skeletal α-actin, which are known to be upregulated in the hypertrophied myocardium. In the PO group, 52 genes were selectively upregulated and 41 genes were downregulated. In the VO group, 88 genes were selectively upregulated and 46 genes were downregulated.

Subsequently, we performed hierarchical clustering with the average linkage method. Figure 4 shows the cluster of upregulated genes (A) and downregulated genes (B) in both hypertrophy groups. The differentially expressed genes were grouped by functional category classification according to the GeneOntology (http://www.geneontology.org/) terms based on the NCBI LocusLink (http://www.ncbi.nlm.nih.gov/LocusLink/) database. The gene cluster that showed the most marked increase was the natriuretic peptide family. The hydrogen-transporting two-sector ATPase group, the cytoskeletal organization and biogenesis group, and the mitochondrial substrate carrier group were upregulated in both hypertrophied hearts. On the other hand, the calcium ion–binding group and the basic-leucine zipper transcription factor group were downregulated in both hypertrophy groups. We observed selective upregulation of the genes that bind to actin in the VO group (*e.g.*, tropomyosin 4, thymosin β-4, and transgelin).

Next, we performed real-time RT-PCR analysis to confirm the results of the DNA chip analysis (Fig. 5). Real-time RT-PCR revealed that BNP, MT and LOXL mRNAs were all upregulated in both the VO and PO groups, compared with the sham group. MT mRNA expression in the VO group was significantly higher than that in the PO group. The levels of BNP and LOXL mRNAs in the VO group were also higher than those in the PO group, but these differences did not reach the level of statistical significance. DNA chip analysis showed that GMP reductase mRNA was selectively downregulated in the VO group. This was confirmed by real-time RT-PCR.

We then examined the expressions of some of the genes that were differentially altered in VO and PO hearts. DNA

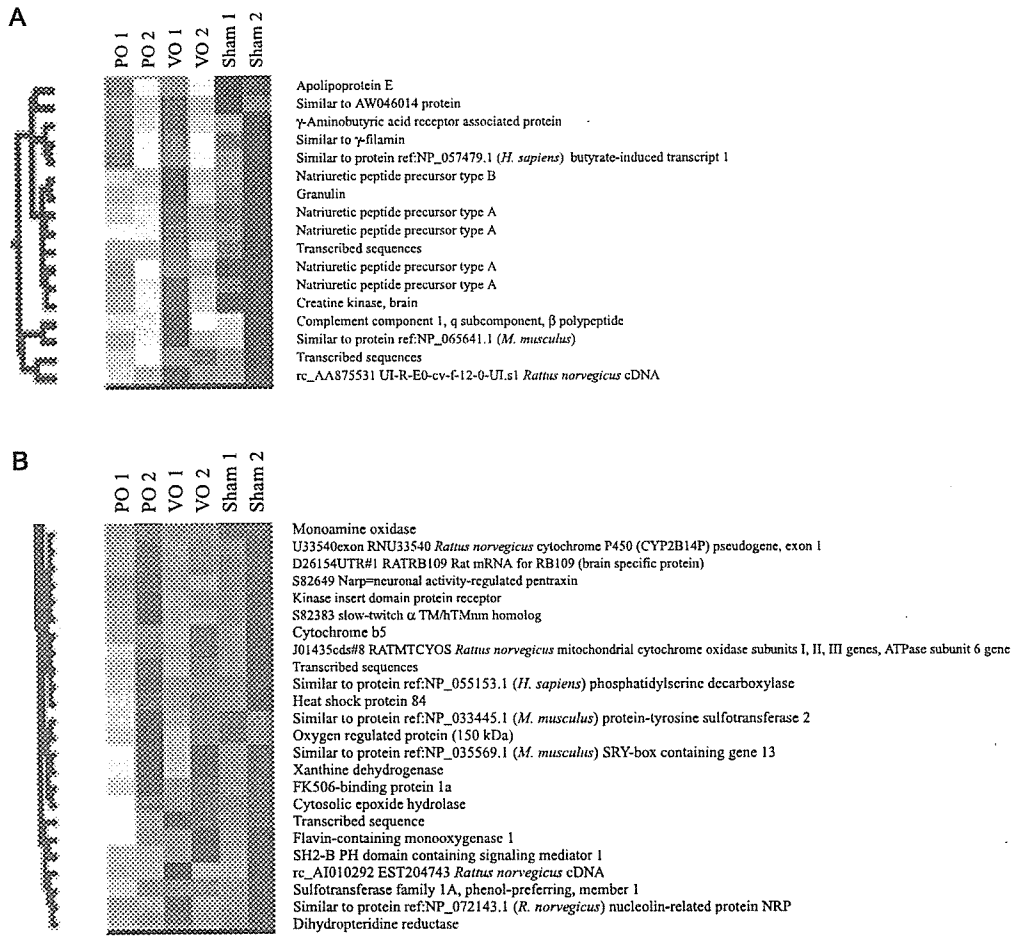

Fig. 4. *Hierarchical cluster analysis of expression profiles. Regulated genes are depicted using a color scale (red, upregulated genes; blue, downregulated genes). A: The one of the cluster consisting of genes that were increased in both forms of hypertrophy. B: The one of the cluster consisting of genes that were decreased in both forms of hypertrophy.*

chip analysis revealed that transgelin was increased in the VO group but downregulated in the PO group, and PDK1 was decreased in VO but upregulated in PO. Real-time RT-PCR confirmed these changes (Fig. 5E, F).

In our DNA chip analysis, BNP and ANP showed the most remarkable upregulations in hypertrophied LVs. MT showed the next highest level of upregulation. Accordingly, we examined the role of MT in the development of cardiac hypertrophy (Fig. 6). MT is a free radical scavenger and is suggested to play a protective role in many cell types. Therefore, we hypothesized that MT plays an anti-apoptotic role in cardiac hypertrophy and performed the following experiments. MT cDNA or control vector (pcDNA3.1) was overexpressed in H9c2 cells. The cells were then exposed to a high concentration of NE for 24 h, and TUNEL staining was performed. In cells overexpressing the control vector, NE increased TUNEL-positive cells. Overexpression of MT inhibited the increase of TUNEL-positive cells (Fig. 6). To confirm the anti-apoptotic effects of MT, we next examined the level of caspase-3 activity, which is critically involved in apoptosis, in these cells (Fig. 7). Caspase-3 activity was increased in cells treated with NE. The overexpression of MT reduced the augmentation of caspase-3 activity by 42±9.9% compared with that in the cells transfected with the control vector (pCDNA3.1; Fig. 7).

Discussion

We examined the similarity and difference of the gene expression profiling between the PO and VO hearts. We found many genes that are regulated similarly or differentially between the two groups. The alterations of some specific genes were confirmed by real-time RT-PCR. Among the genes that were upregulated in both forms of hypertrophy, we examined the role of MT in apoptosis, and found that this gene played a novel role in anti-apoptosis.

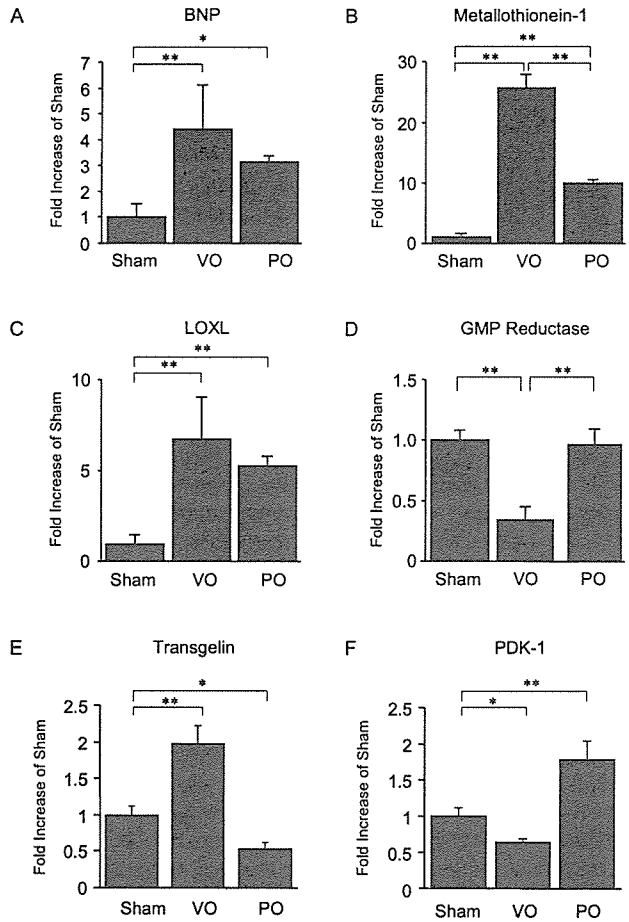

Fig. 5. *Real-time RT-PCR. A: B-type natriuretic peptide (BNP). B: Metallothionein-1 (MT). C: Lysyl oxidase–like protein 1 (LOXL). D: GMP reductase. E: Transgelin. F: Pyruvate dehydrogenase kinases-1 (PDK-1). Values are the mean±SD.* *p < 0.05, **p < 0.01.

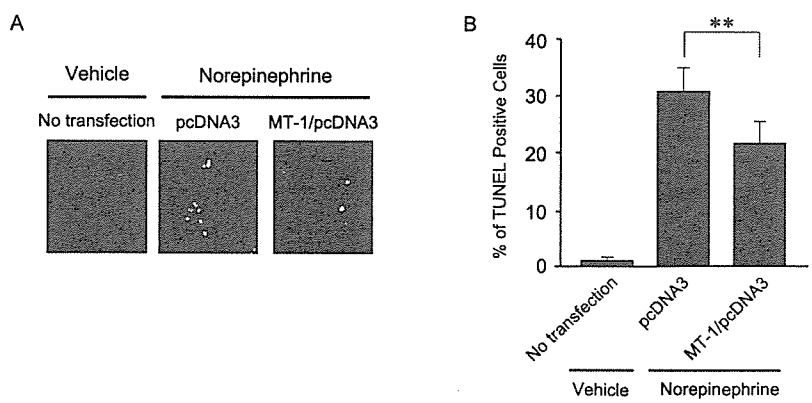

Fig. 6. *Effects of overexpression of MT on the percentage of TUNEL-positive cells. A: TUNEL staining. B: Percentage of TUNEL-positive cells. H9c2 cells were transfected with MT-pcDNA3 or pcDNA3 alone. At 24 h after the transfection, cells were exposed to norepinephrine (10^{-4} mol/l) and cultured for an additional 24 h. TUNEL staining was performed as described in Methods. Values are the mean±SD.* **p < 0.01.

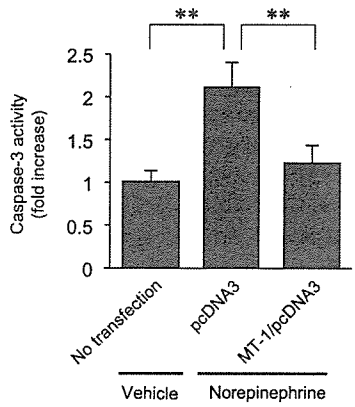

Fig. 7. *Effects of overexpression of MT on caspase-3 activity. H9c2 cells were transfected with MT-pcDNA3 or pcDNA3 alone. At 24 h after the transfection, cells were exposed to norepinephrine (10^{-4} mol/l) and cultured for an additional 24 h. The caspase-3 assay was performed as described in Methods. Data are from four independent experiments. Values are the mean±SD.* **$p < 0.01$.

Methodological Considerations

In this study, we used two different procedures to induce cardiac hypertrophy: abdominal constriction for pressure overload and aortocaval shunt for volume overload. These two procedures produced the same magnitude of hypertrophy with distinct morphological differences as shown by echocardiography. Thus the similarities in gene profiling may be attributable to hypertrophy *per se* and the dissimilarity to the different morphologies of the heart, *i.e.*, concentric hypertrophy or eccentric hypertrophy. In both forms of hypertrophy, cardiac function assessed by fractional shortening was normal, indicating that changes in gene profiling were not attributable to those of the myocardium at the failing stage.

These mechanical stresses activate many molecules in the heart. There are two peaks in the activations of biochemical signals after an exposure to hemodynamic load (*18*). Acute responses occur within a few minutes, and hypertrophic responses follow over the next several days or weeks. As a pilot study, we measured the time-dependent change of the expression of BNP mRNA in rat PO hearts. The left ventricular weight/body weight ratio increased gradually until day 28 after the initiation of PO and continued at a plateau level thereafter. BNP mRNA levels showed a biphasic response, *i.e.*, an initial increase and a later gradual increase. The first peak of the expression was at 24 h and the subsequent peak was at day 28 (data not shown). Thus, at day 28 acute gene responses were no longer observed and hypertrophic gene responses were maximal and stable. This is the time when hypertrophy was morphologically established. In order to investigate gene responses with hypertrophy but without heart failure, we chose day 28.

We examined gene profiling at the stage of established cardiac hypertrophy but did not examine it chronologically. Thus the gene profiling in our study may not represent that of the developmental stage of hypertrophy, but merely that of the compensation of hypertrophy. Moreover, we examined gene profiling of the whole heart. Thus our results do not necessarily indicate gene profiling of cardiomyocytes, but may also include profiling for the interstitial tissues.

Gene Profiling in PO and VO

The present study revealed gene expression profiles that may be associated with hypertrophy *per se* or different types of remodeling. In agreement with previous reports (*13*, *14*, *19*, *20*), we found changes in gene profiling in PO. As shown in Fig. 3, most genes were unaltered in the hypertrophic myocardium induced by PO. Only 85 genes were upregulated. Thus, the number of genes upregulated in the hypertrophied myocardium induced by PO was less than that of several previous reports. This discrepancy may be ascribable to the criteria used for the gene selection and the use of different kinds of chips. The present study is the first to describe gene expressions in VO. As shown in Fig. 3 and Table 1, the levels of most of the genes were unaltered, just as in PO. Only 121 genes were upregulated. It may be interesting to note that some genes were regulated differentially between VO and PO. Among those genes, extracellular matrix–related proteins, *e.g.*, osteopontin, secreted acidic cysteine rich glycoprotein, and tropoelastin, were predominantly upregulated in VO. The upregulation of these genes may be related to the specific remodeling in VO, but not to hypertrophy *per se*. In addition, the selective upregulation of genes in VO that bind to actin (*e.g.*, tropomyosin 4, thymosin β-4, and transgelin) may explain the difference in structural ventricular remodeling between VO and PO. Several gene profiles have been reported in other models of hypertrophy (*21*, *22*). These reports have shown that the common genetic events in hypertrophy include upregulations of ANP, BNP, and skeletal α-actin. These genes were increased in both forms of hypertrophy in the present study as well.

GMP reductase was predominantly downregulated in VO. Because GMP reductase increases the adenine nucleotide pool through synthesis of inosine monophosphate (*23*), the decrease of GMP reductase may have some deteriorative effects on myocardial metabolism. We also found that the expressions of PDK-1 and transgelin were differentially regulated in VO and PO hearts (Fig. 5E, F). Transgelin (also known as SM22 α) is a 22-kDa protein that is associated with cytoskeletal actin filament bundles in contractile smooth muscle cell (SMC) (*24*, *25*). It is expressed in cardiac, smooth, and skeletal muscle cells during early embryogenesis but becomes restricted to visceral and vascular SMC at late embryonic stages and throughout adulthood. Transgelin was upregulated in VO and downregulated in PO hearts in the

present study (Fig. 5E), but the significance of these changes is unknown. Transgelin may regulate several genes that are associated with vascular development, remodeling, and alterations. The differential expression of this gene may reflect the difference of vascular remodeling between concentric and eccentric cardiac hypertrophy. PDK-1 was downregulated in VO but upregulated in PO (Fig. 5F). PDKs phosphorylate the mitochondrial pyruvate dehydrogenase complex, which catalyzes the oxidative decarboxylation of pyruvate, and thereby inactivate it (*26*). Although the significance of alterations of this enzyme in the hypertrophied hearts is unclear, these changes may be associated with the difference of the myocardial energy production in both forms of hypertrophy.

Upregulated Genes in Both Forms of Hypertrophy

Our DNA chip analysis showed upregulation of 33 genes in both forms hypertrophy (Table 1). These genes may be associated with hypertrophy *per se*. Among these genes, we confirmed the upregulations of BNP, MT and LOXL mRNA. Wang *et al.* (*13*) and Weinberg *et al.* (*14*) have reported that MT is upregulated significantly in aortic banding mice. In the present study, MT was one of genes showing the highest level of upregulation in both forms of hypertrophied heart. Accordingly, we examined the role of MT in cardiac hypertrophy. MT is a cysteine-rich protein with a strong affinity for Zn^{2+} (reviewed in Palmitter (*27*), and Kang (*28*)). MT is known to detoxify the heavy metals. Recent studies revealed that MT binds to rare metals *in vivo* and regulates metalprotein and metal-dependent transcriptional factors. Moreover, MT is a potent free radical scavenger. And in the hearts of mice with adriamycin-induced cardiomyopathy, MT expression has been shown to be increased (*29*). Moreover, it has been reported that overexpression of MT in the hearts of transgenic mice suppresses doxorubicin cardiotoxicity and ischemia-reperfusion injury (*30*, *31*). Thus MT plays cytoprotective roles in many cell types. In this study, MT suppressed the NE-induced increase of TUNEL-positive cells. This inhibition was associated with the suppression of caspase-3 activity, suggesting that MT inhibits the apoptosis of cardiomyocytes. It has been reported that the myocardium of both rat models of hypertrophy shows apoptotic cardiomyocyte death (*32*, *33*). Therefore, we consider that MT may exert anti-apoptotic effects under physiological conditions. Aronow and coworkers showed that MT was universally increased in hypertrophied hearts produced by four different mechanisms, suggesting that the upregulation of MT is a highly conserved genetic event in hypertrophy (*21*). Interestingly, the expression of MT was greater in the hypertrophy model than in the heart failure model in their study (*21*). This suggests that apoptosis of the hypertrophied myocardium, which leads to heart failure, is prevented by the expression of MT. Taken together, these findings indicate that MT may have a protective effect on the heart through its anti-apoptotic effects.

LOXL was also significantly upregulated in both forms of hypertrophy. LOXL is a member of the lysyl oxidase gene family, which is an extracellular, copper-dependent enzyme family that initiates the cross-linking of collagens and elastin (*34*, *35*). It may be possible that LOXL is associated with the remodeling of the extracellular matrix in the hypertrophied myocardium. Among the upregulated genes, GATA-4 is known to be essential for the induction of several cardiac-specific genes (*36*). The upregulation of GATA-4 supports the idea that this protein may be the common regulator of hypertrophic responses.

In conclusion, we found many genes that are similarly or dissimilarly regulated in the hearts of VO and PO. The altered expressions of BNP, MT, GMP reductase, LOXL, transgelin, and PDK-1 were confirmed by real-time RT-PCR. Gene profiling by DNA chip technology represents a useful tool for identification of genes that may contribute to morphological and functional differences between PO and VO. Moreover, the overexpression of MT in H9c2 cells attenuated the norepinephrine-induced apoptosis. MT may play a novel protective role in the development of cardiac hypertrophy. Although we found that many genes were altered in the hypertrophied hearts, it remains uncertain whether these changes played a role in or were secondary to the development of hypertrophy. To clarify these questions, functional studies should be performed for each molecule.

Acknowledgements

We thank Yumika Tamoto for valuable technical assistance.

References

1. Lorell BH, Carabello BA: Left ventricular hypertrophy: pathogenesis, detection, and prognosis. *Circulation* 2000; **102**: 470–479.
2. Hunter JJ, Chien KR: Signaling pathways for cardiac hypertrophy and failure. *N Engl J Med* 1999; **341**: 1276–1283.
3. Homcy CJ: Signaling hypertrophy: how many switches, how many wires. *Circulation* 1998; **97**: 1890–1892.
4. Diamond JA, Phillips RA: Hypertensive heart disease. *Hypertens Res* 2005; **28**: 191–202.
5. Chapman D, Weber KT, Eghbali M: Regulation of fibrillar collagen types I and III and basement membrane type IV collagen gene expression in pressure overloaded rat myocardium. *Circ Res* 1990; **67**: 787–794.
6. Namba T, Tsutsui H, Tagawa H, *et al*: Regulation of fibrillar collagen gene expression and protein accumulation in volume-overloaded cardiac hypertrophy. *Circulation* 1997; **95**: 2448–2454.
7. Nagatomo Y, Carabello BA, Coker ML, *et al*: Differential effects of pressure or volume overload on myocardial MMP levels and inhibitory control. *Am J Physiol Heart Circ Physiol* 2000; **278**: H151–H161.
8. Imamura T, McDermott PJ, Kent RL, Nagatsu M, Cooper G 4th, Carabello BA: Acute changes in myosin heavy chain synthesis rate in pressure *versus* volume overload. *Circ Res*

1994; **75**: 418–425.
9. Yoshihara F, Nishikimi T, Horio T, *et al*: Ventricular adrenomedullin concentration is a sensitive biochemical marker for volume and pressure overload in rats. *Am J Physiol Heart Circ Physiol* 2000; **278**: H633–H642.
10. Calderone A, Takahashi N, Izzo NJ Jr, Thaik CM, Colucci WS: Pressure- and volume-induced left ventricular hypertrophies are associated with distinct myocyte phenotypes and differential induction of peptide growth factor mRNAs. *Circulation* 1995; **92**: 2385–2390.
11. Modesti PA, Vanni S, Bertolozzi I, *et al*: Early sequence of cardiac adaptations and growth factor formation in pressure- and volume-overload hypertrophy. *Am J Physiol Heart Circ Physiol* 2000; **279**: H976–H985.
12. Tsutsui H, Tagawa H, Kent RL, *et al*: Role of microtubules in contractile dysfunction of hypertrophied cardiocytes. *Circulation* 1994; **90**: 533–555.
13. Wang D, Oparil S, Feng JA, *et al*: Effects of pressure overload on extracellular matrix expression in the heart of the atrial natriuretic peptide-null mouse. *Hypertension* 2003; **42**: 88–95.
14. Weinberg EO, Mirotsou M, Gannon J, Dzau VJ, Lee RT, Pratt RE: Sex dependence and temporal dependence of the left ventricular genomic response to pressure overload. *Physiol Genomics* 2003; **12**: 113–127.
15. Limas CJ: Increased number of beta-adrenergic receptors in the hypertrophied myocardium. *Biochim Biophys Acta* 1979; **588**: 174–178.
16. Garcia R, Diebold S: Simple, rapid, and effective method of producing aortocaval shunts in the rat. *Cardiovasc Res* 1990; **24**: 430–432.
17. Li C, Wong WH: Model-based analysis of oligonucleotide arrays: expression index computation and outlier detection. *Proc Natl Acad Sci U S A* 2001; **98**: 31–36.
18. Hoshijima M, Chien KR: Mixed signals in heart failure: cancer rules. *J Clin Invest* 2002; **109**: 849–855.
19. Kong SW, Bodyak N, Yue P, *et al*: Genetic expression profiles during physiological and pathological cardiac hypertrophy and heart failure in rats. *Physiol Genomics* 2005; **21**: 34–42.
20. Ueno S, Ohki R, Hashimoto T, *et al*: DNA microarray analysis of *in vivo* progression mechanism of heart failure. *Biochem Biophys Res Commun* 2003; **307**: 771–777.
21. Aronow BJ, Toyokawa T, Canning A, *et al*: Divergent transcriptional responses to independent genetic causes of cardiac hypertrophy. *Physiol Genomics* 2001; **6**: 19–28.
22. Friddle CJ, Koga T, Rubin EM, Bristow J: Expression profiling reveals distinct sets of genes altered during induction and regression of cardiac hypertrophy. *Proc Natl Acad Sci U S A* 2000; **97**: 6745–6750.
23. Zoref-Shani E, Shirin C, Sidi Y, Bromberg Y, Sperling O: Metabolism of guanine and guanine nucleotides in primary rat cardiomyocyte cultures. *Biochem Mol Med* 1995; **55**: 149–155.
24. Feil S, Hofmann F, Feil R: SM22alpha modulates vascular smooth muscle cell phenotype during atherogenesis. *Circ Res* 2004; **94**: 863–865.
25. Morgan KG, Gangopadhyay SS: Invited review: cross-bridge regulation by thin filament–associated proteins. *J Appl Physiol* 2001; **91**: 953–962.
26. Sugden MC, Holness MJ: Recent advances in mechanisms regulating glucose oxidation at the level of the pyruvate dehydrogenase complex by PDKs. *Am J Physiol Endocrinol Metab* 2003; **284**: E855–E862.
27. Palmiter RD: The elusive function of metallothioneins. *Proc Natl Acad Sci U S A* 1998; **95**: 8428–8430.
28. Kang YJ: The antioxidant function of metallothionein in the heart. *Proc Soc Exp Biol Med* 1999; **222**: 263–273.
29. Yin X, Wu H, Chen Y, Kang YJ: Induction of antioxidants by adriamycin in mouse heart. *Biochem Pharmacol* 1998; **56**: 87–93.
30. Kang YJ, Chen Y, Yu A, Voss-McCowan M, Epstein PN: Overexpression of metallothionein in the heart of transgenic mice suppresses doxorubicin cardiotoxicity. *J Clin Invest* 1997; **100**: 1501–1506.
31. Kang YJ, Li Y, Sun X: Antiapoptotic effect and inhibition of ischemia/reperfusion-induced myocardial injury in metallothionein-overexpressing transgenic mice. *Am J Pathol* 2003; **163**: 1579–1586.
32. Teiger E, Than VD, Richard L, *et al*: Apoptosis in pressure overload–induced heart hypertrophy in the rat. *J Clin Invest* 1996; **97**: 2891–2897.
33. Cox MJ, Sood HS, Hunt MJ, *et al*: Apoptosis in the left ventricle of chronic volume overload causes endocardial endothelial dysfunction in rats. *Am J Physiol Heart Circ Physiol* 2002; **282**: H1197–H1205.
34. Kagan HM, Li W: Lysyl oxidase: properties, specificity, and biological roles inside and outside of the cell. *J Cell Biochem* 2003; **88**: 660–672.
35. Bank RA, van Hinsbergh VW: Lysyl oxidase: new looks on LOX. *Arterioscler Thromb Vasc Biol* 2002; **22**: 1365–1366.
36. Molkentin JD: The zinc finger-containing transcription factors GATA-4, -5, and -6. Ubiquitously expressed regulators of tissue-specific gene expression. *J Biol Chem* 2000; **275**: 38949–38952.

Significance of Asymmetric Basal Posterior Wall Thinning in Patients With Cardiac Fabry's Disease

Makoto Kawano, MD[a], Toshihiro Takenaka, MD[a], Yutaka Otsuji, MD[a,*], Hiroyuki Teraguchi, MD[a], Shiro Yoshifuku, MD[a], Toshinori Yuasa, MD[a], Bo Yu, MD[a], Masaaki Miyata, MD[a], Shuichi Hamasaki, MD[a], Shinichi Minagoe, MD[a], Yuichi Kanmura, MD[b], and Chuwa Tei, MD[a]

Although classic Fabry's disease results in multiple causes of death, the cardiac variant of Fabry's disease affects only the cardiac system and results in initial symmetric left ventricular (LV) hypertrophy and later LV dysfunction, asymmetric basal posterior LV wall thinning, restrictive mitral flow, and functional mitral regurgitation with end-stage chronic heart failure (CHF), leading to death. The purpose of this study was to investigate whether these findings predict prognoses in patients with cardiac Fabry's disease. In 13 consecutive men with cardiac Fabry's disease, LV wall thickness, the ejection fraction, mitral E-wave deceleration time, the LV Tei index, and functional mitral regurgitation were measured by echocardiography. Patients were followed for 5 to 96 months (mean 41 ± 9). Eight patients developed New York Heart Association class III CHF, and 6 experienced cardiac death. A LV Tei index >0.60 and basal posterior LV wall thinning with a ratio of ventricular septal to posterior wall thickness >1.3 significantly preceded CHF and death (Tei index: 4.4 and 5.1 years; posterior wall thinning: 4.0 and 4.7 years), respectively ($p < 0.05$). In conclusion, an increased LV Tei index and asymmetric basal posterior LV wall thinning are important echocardiographic findings that precede CHF and cardiac death in patients with cardiac Fabry's disease. **(Am J Cardiol 2007;99:261–263)**

Patients with classic Fabry's disease show multiple organ involvement, leading to heterogenous causes of death.[1,2] In contrast, an atypical variant of Fabry's disease with manifestations limited to the heart, reported as cardiac Fabry's disease,[3,4] is more frequent than previously expected and can be found in 3% to 6% of men with left ventricular (LV) hypertrophy.[5,6] We have empirically observed that patients with cardiac Fabry's disease initially present with symmetric LV hypertrophy without chronic heart failure (CHF) but later show LV dysfunction, asymmetric LV basal posterior wall thinning without ventricular septal thinning, restrictive mitral flow, and functional mitral regurgitation with end-stage CHF and cardiac death. The purpose of this study was to investigate the natural history of these findings and to characterize predictors of New York Heart Association (NYHA) class III CHF or cardiac death in patients with cardiac Fabry's disease.

Methods and Results

Four hundred fifty consecutive patients with ventricular septal or posterior wall thickness ≥13 mm were screened by the measurement of plasma α-galactosidase A activity from 1992 to 1996 at our institution, and 13 men were diagnosed with cardiac Fabry's disease using the following criteria:

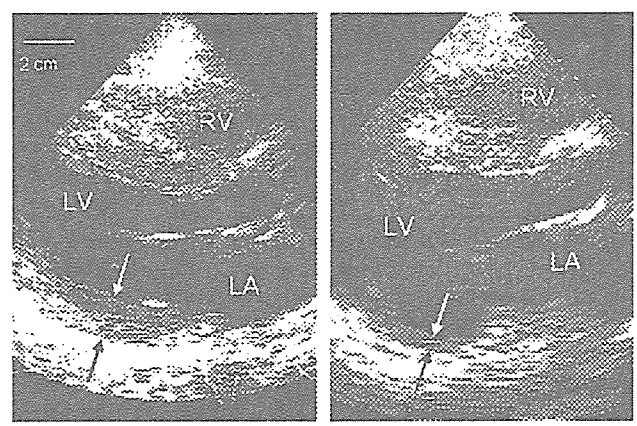

Figure 1. Serial echocardiograms of a patient with cardiac Fabry's disease at 57 *(left)* and 63 *(right)* years old. Ventricular septal and posterior wall thicknesses changed from 21 and 18 to 19 and 7 mm, respectively, with the development of CHF. LA = left atrium; LV = left ventricle; RV = right ventricle.

(1) low plasma α-galactosidase A activity (<4.5 nmol/hour/ml)[5]; (2) ventricular septal and/or posterior wall thickness ≥13 mm; (3) no clinical features of classic Fabry's disease, including angiokeratoma, acroparesthesia, hypohidrosis, and corneal opacity; and (4) accumulation of glycosphingolipid in biopsied cardiomyocytes and/or α-galactosidase A gene abnormalities.[7] These patients were followed for 41 ± 9 months by serial echocardiography, with intervals of 1 to 24 months (mean 3.3 ± 1.1). Clinical profiles are listed in Table 1. Coronary angiographic results were normal, and written informed consent was obtained from all patients.

Ventricular septal and posterior wall thicknesses were

Departments of [a]Cardiovascular, Respiratory and Metabolic Medicine and [b]Anesthesiology and Critical Care Medicine, Graduate School of Medicine, Kagoshima University, Kagoshima, Japan. Manuscript received January 23, 2006; revised manuscript received and accepted July 27, 2006.

*Corresponding author: Tel: 81-99-275-5318; fax: 81-99-265-8447.
E-mail address: otsujiy@med.uoeh-u.ac.jp (Y. Otsuji).

0002-9149/07/$ – see front matter
doi:10.1016/j.amjcard.2006.07.088

Table 1
Clinical, enzymatic, pathologic, and genetic characteristics of patients

No.	Age at Diagnosis (yrs)	Previous Diagnosis	Plasma α-gal A Activity (nmol/h/ml)	Accumulation in Myocyte	Gene Abnormality	Age at NYHA Class III (yrs)	Duration of Follow-Up (mo)	Age at Death (yrs)
1	47	HC	1.5	+	NE	NYHA <III	20	Alive
2	57	HC	0.4	+	A20P	62	85	64
3	60	HC	1.0	0	F229L	NYHA <III	16	Alive
4	62	HC	1.2	+	Decreased mRNA	67	76	68
5	62	HC	1.3	+	NE	63	25	64
6	66	HC	0.9	+	NE	66	7	66
7	70	HC	0.6	+	Decreased mRNA	73	40	74
8	71	HC	1.4	+	NE	73	46	Alive
9	71	HC	0.7	+	Decreased mRNA	75	55	76
10	74	HC	1.0	+	NE	NYHA <III	6	Alive
11	79	HC	0.6	NE	Decreased mRNA	80	96	Alive
12	43	HHD	1.1	+	NE	NYHA <III	5	Alive
13	62	HHD	0.6	+	M296I	NYHA <III	58	Alive

α-gal A = α-galactosidase A; HC = hypertrophic cardiomyopathy; HHD = hypertensive heart disease; mRNA = messenger ribonucleic acid; NE = not examined.

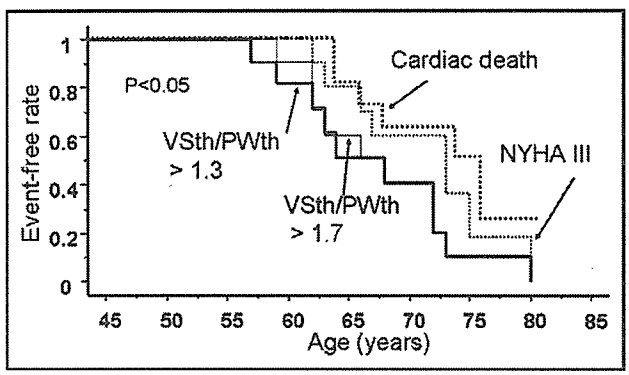

Figure 2. Kaplan-Meier curves showing that ventricular septum/posterior wall thickness ratio (VSth/PWth) >1.3 and 1.7 significantly preceded NYHA class III CHF and cardiac death in patients with cardiac Fabry's disease.

measured with echocardiography, and their ratio was calculated, with 1.2 defined as the upper limit of normal.[8] The LV ejection fraction was measured by the biplane Simpson's method, and left atrial dimension was measured by M-mode echocardiography. A mitral flow restrictive filling pattern was defined as an E/A ratio >2 and E-wave deceleration time <150 ms.[9] The Tei index, combining systolic and diastolic function, was obtained by mitral filling and aortic ejection flow.[10] Mitral regurgitant volume was quantified by Doppler echocardiography.

Statistical analysis was performed using StatView version 5.0 (SAS Institute Inc., Cary, North Carolina). Clinical and echocardiographic data after the introduction of enzymatic replacement therapy were excluded from analysis. The event-free rate from the ventricular septum/posterior wall thickness ratio >1.3, 1.5, 1.7, or 1.9; LV ejection fraction <50%; left atrial dimension >40 mm; restrictive mitral flow; Tei index >0.50, 0.60, 0.70, or 0.80; mitral regurgitant fraction >30%; NYHA class III; and cardiac death was calculated using the Kaplan-Meier method. A p value <0.05 was considered significant.

NYHA class III or IV CHF developed in 8 of the 13 patients during follow-up. Six died, and the cause was CHF in all 6 patients. Most patients with CHF demonstrated (1) LV systolic and diastolic dysfunction, with reduced ejection fractions, shortened mitral E-wave deceleration times, and increased Tei indexes; (2) left atrial dilation; (3) asymmetric basal posterior LV wall thinning (Figure 1); and (4) significant mitral regurgitation. The ages at the development of these findings are listed in Table 2.

Among the evaluated echocardiographic events, Kaplan-Meier analysis identified significant associations with progression to NYHA class III CHF and cardiac death for a Tei index >0.60 and ventricular septum/posterior wall thickness ratio >1.3, 1.5, and 1.7 (Figure 2). A Tei index >0.60 preceded NYHA class III CHF and death by 4.4 and 5.1 years ($p < 0.05$), respectively. Ventricular septum/posterior wall thickness ratio >1.3, 1.5, or 1.7 significantly preceded NYHA class III CHF and cardiac death by 4.0, 3.8, or 3.4 and 4.7, 4.5, or 4.1 years ($p < 0.05$), respectively.

Discussion

This study demonstrated that an increased Tei index and LV basal posterior wall thinning were significantly associated with progression to NYHA class III CHF and cardiac death in patients with cardiac Fabry's disease. Other findings, such as a reduced LV ejection fraction, restrictive mitral flow, left atrial dilation, and significant mitral regurgitation, occurred temporally close to the development of CHF or cardiac death and were unable to predict disease progression by Kaplan-Meier analysis. These results may lead to a better understanding of the natural history of cardiac Fabry's disease and better timing to start enzymatic replacement or gene therapy.[11–14]

The Tei index enables the prediction of outcomes in patients with cardiac amyloidosis and other diseases.[15] Basal posterior LV wall thinning and fibrosis have also been reported in patients with cardiac involvement in classic Fabry's disease.[16,17] The findings of the present study are consistent with these and further demonstrate that an increased Tei index and asymmetric LV basal posterior wall thinning are associated with progression to

Table 2
Age at event occurrence

No.	Echocardiographic Events												Clinical Events	
	LV Tei Index				VS/PW				LAD	LVEF	Restrictive	MR Fraction	NYHA	Cardiac
	>0.50	>0.60	>0.70	>0.80	>1.3	>1.5	>1.7	>1.9	>40 mm	<50%	Mitral Flow	>30%	Class III	Death
1	49	49	NE	NE	NE	NE	NE	NE	49	NE	NE	NE	NE	NE
2	57	60	60	60	59	59	59	60	59	59	62	62	62	64
3	60	60	60	NE	NE	NE	NE	NE	NE	NE	NE	NE	NE	NE
4	65	65	65	67	63	63	63	63	66	63	66	68	67	68
5	62	62	62	62	57	57	62	62	62	62	63	64	63	64
6	66	66	66	66	64	66	66	66	66	66	66	66	66	66
7	73	73	73	73	73	73	73	73	73	73	73	73	73	74
8	72	72	73	73	68	68	68	71	73	71	73	NE	73	NE
9	75	75	75	75	72	72	72	72	75	75	75	75	75	76
10	74	74	74	NE	72	72	72	NE	74	74	NE	NE	NE	NE
11	80	80	80	NE	80	80	80	80	80	80	80	NE	80	NE
12	43	NE	NE	NE	NE	NE	NE	NE	43	NE	NE	NE	NE	NE
13	66	66	NE	NE	62	62	66	66	NE	66	NE	NE	NE	NE
Mean	64.8	66.8	69.4	70.0	67.2	67.4	67.8	69.4	68.3	69.0	70.6	70.7	71.2	71.9
SE	3.0	2.5	2.1	1.9	2.2	2.2	2.0	2.2	2.9	2.1	2.0	1.7	2.1	1.7

Means and SEs were obtained by the Kaplan-Meier method.

EF = ejection fraction; LAD = left atrial dimension; MR = mitral regurgitation; NE = no event throughout the observation; PW = posterior wall thickness; VS = ventricular septal thickness.

CHF and cardiac death in patients with cardiac Fabry's disease.

Although the incidence of cardiac Fabry's disease is more common than previously believed,[5,6] its incidence and the utility of screening in patients with LV hypertrophy need to be established with a large number of patients. A Tei index >0.60 and LV basal posterior wall thinning were associated with progression to CHF and cardiac death in patients with cardiac Fabry's disease, whose causes of death were uniformly cardiac. However, the results may not be generalized to classic Fabry's disease with heterogenous causes of death. Tissue Doppler imaging and the Tei index may allow the earlier and better prediction of cardiac Fabry's disease before the development of structural abnormalities,[18] which requires further investigation.

1. Desnick RJ, Ioannou YA, Eng CM. α-Galactosidase A deficiency: Fabry disease. In: Scriver CR, Beaudet AL, Sly WS, Valle D, eds. The Metabolic and Molecular Basis of Inherited Disease, Vol. 3. 8th Ed. New York, New York: McGraw-Hill, 2001:3733–3774.
2. Desnick RJ, Brady R, Barranger J, Collins AJ, Germain DP, Goldman M, Grabowski G, Packman S, Wilcox WR. Fabry disease, an under-recognized multisystemic disorder: expert recommendations for diagnosis, management, and enzyme replacement therapy. *Ann Intern Med* 2003;138:338–346.
3. Elleder M, Bradová V, Šmíd F, Budešínsky, M, Harzer K, Kustermann-Kuhn B, Ledvinova J, Belohlavek, Kral V, Dorazilova V. Cardiocyte storage and hypertrophy as a sole manifestation of Fabry's disease. Report on a case simulating hypertrophic non-obstructive cardiomyopathy. *Virchows Arch A Pathol Anat Histopathol* 1990;417:449–455.
4. von Scheidt W, Eng CM, Fitzmaurice TF, Erdmann E, Hübner G, Olsen EGJ, Christomanou H, Kandolf R, Bishop DF, Desnick RJ. An atypical variant of Fabry's disease with manifestations confined to the myocardium. *N Engl J Med* 1991;324:395–399.
5. Nakao S, Takenaka T, Maeda M, Kodama C, Tanaka A, Tahara M, Yoshida A, Kuriyama M, Hayashibe H, Sakuraba H, Tanaka H. An atypical variant of Fabry's disease in men with left ventricular hypertrophy. *N Engl J Med* 1995;333:288–293.
6. Sachdev B, Takenaka T, Teraguchi H, Tei C, Lee P, McKenna WJ, Elliott PM. Prevalence of Anderson-Fabry disease in male patients with late onset hypertrophic cardiomyopathy. *Circulation* 2002;105:1407–1411.
7. Yoshitama T, Nakao S, Takenaka T, Teraguchi H, Sasaki T, Kodama C, Tanaka A, Kisanuki A, Tei C. Molecular genetic, biochemical, and clinical studies in three families with cardiac Fabry's disease. *Am J Cardiol* 2001;87:71–75.
8. Henry WL, Clark CE, Epstein SE. Asymmetric septal hypertrophy: echocardiographic identification of the pathognomonic anatomic abnormality of IHSS. *Circulation* 1973;47:225–233.
9. Cohen GI, Pietrolungo JF, Thomas JD, Klein AL. A practical guide to assessment of ventricular diastolic function using Doppler echocardiography. *J Am Coll Cardiol* 1996;27:1753–1760.
10. Tei C. New non-invasive index for combined systolic and diastolic ventricular function. *J Cardiol* 1995;26:135–136.
11. Eng CM, Guffon N, Wilcox WR, Germain DP, Lee P, Waldek S, Caplan L, Linthorst GE, Desnick RJ. Safety and efficacy of recombinant human α-galactosidase A replacement therapy in Fabry's disease. *N Engl J Med* 2001;345:9–16.
12. Schiffmann R, Murray GJ, Treco D, Daniel P, Sellos-Moura M, Myers M, Quirk JM, Zirzow E, Liang TJ, Kreps C, et al. Infusion of alpha-galactosidase A reduces tissue globotriaosylceramide storage in patients with Fabry disease. *Proc Natl Acad Sci USA* 2000;97:365–370.
13. Takenaka T, Murray GJ, Qin G, Quirk JM, Ohshima T, Qasba P, Clark K, Kulkarni AB, Brady RO, Medin JA. Long-term enzyme correction and lipid reduction in multiple organs of primary and secondary transplanted Fabry mice receiving transduced bone marrow cells. *Proc Natl Acad Sci U S A* 2000;97:7515–7520.
14. Yoshimitsu M, Sato T, Tao K, Walia JS, Rasaiah VI, Sleep GT, Murray GJ, Poeppl AG, Underwood J, West L, et al. Bioluminescent imaging of a marking transgene and correction of Fabry mice by neonatal injection of recombinant lentiviral vectors. *Proc Natl Acad Sci USA* 2004;101:16909–16914.
15. Tei C, Dujardin KS, Hodge DO, Kyle RA, Tajik AJ, Seward JB. Doppler index combining systolic and diastolic myocardial performance: clinical value in cardiac amyloidosis. *J Am Coll Cardiol* 1996;28:658–664.
16. Bass JL, Shrivastava S, Grabowski GA, Desnick RJ, Moller JH. The M-mode echocardiogram in Fabry's disease. *Am Heart J* 1980;100:807–812.
17. Moon JCC, Sachdev B, Elkington AG, McKenna WJ, Mehta A, Pennell DJ, Leed PJ, Elliott PM. Gadolinium enhanced cardiovascular magnetic resonance in Anderson-Fabry disease: evidence for a disease specific abnormality of the myocardial interstitium. *Eur Heart J* 2003;24:2151–2155.
18. Pieroni M, Chimenti C, Ricci R, Sale P, Russo MA, Frustaci A. Early detection of Fabry cardiomyopathy by tissue Doppler imaging. *Circulation* 2003;107:1978–1984.

American Journal of Pathology, Vol. 168, No. 2, February 2006

DOI: 10.2353/ajpath.2006.050137

Cardiovascular, Pulmonary and Renal Pathology

Autophagic Cardiomyocyte Death in Cardiomyopathic Hamsters and Its Prevention by Granulocyte Colony-Stimulating Factor

Shusaku Miyata,* Genzou Takemura,* Yukinori Kawase,* Yiwen Li,* Hideshi Okada,* Rumi Maruyama,* Hiroaki Ushikoshi,* Masayasu Esaki,* Hiromitsu Kanamori,* Longhu Li,* Yu Misao,* Asaki Tezuka,† Teruhiko Toyo-Oka,† Shinya Minatoguchi,* Takako Fujiwara,‡ and Hisayoshi Fujiwara*

From the Second Department of Internal Medicine, Gifu University School of Medicine, Gifu; the Department of Organ Pathophysiology and Internal Medicine,† University of Tokyo, Tokyo; and the Department of Food Science,‡ Kyoto Women's University, Kyoto, Japan*

In UM-X7.1 hamster model of human dilated cardiomyopathy, heart failure progressively develops and causes 50% mortality by 30 weeks of age. Through ultrastructural analysis, we found that many cardiomyocytes of this model contain typical autophagic vacuoles including degraded mitochondria, glycogen granules, and myelin-like figures. In addition, ubiquitin, cathepsin D, and Rab7 were overexpressed as determined by immunoassays. Importantly, most cardiomyocytes with leaky plasma membranes were positive for cathepsin D, suggesting a direct link between autophagic degeneration and cell death. Meanwhile, cardiomyocyte apoptosis appeared insignificant. Granulocyte colony-stimulating factor (10 μg/kg/day), injected 5 days/week from 15 to 30 weeks of age, improved survival among 30-week-old hamsters (100% versus 53% in the untreated hamsters, $P < 0.0001$); ventricular function and remodeling, increased cardiomyocyte size, and reduced myocardial fibrosis followed by a dramatic reduction in the autophagic findings were also seen. Granulocyte colony-stimulating factor also down-regulated tumor necrosis factor-α and increased activities of Akt signal transducer and activator of transcription-3, and matrix metalloproteinases. However, there was no clear evidence of transdifferentiation from bone marrow cells into cardiomyocytes. In conclusion, autophagic death is important for cardiomyocyte loss in the cardiomyopathic hamster, and the beneficial effect of granulocyte colony-stimulating factor acts mainly via an anti-autophagic mechanism rather than anti-apoptosis or regeneration. *(Am J Pathol 2006, 168:386–397; DOI: 10.2353/ajpath.2006.050137)*

Autophagy was originally defined as the process of sequestration of intracellular components and their subsequent degradation by lysosomal vacuoles.[1] Although autophagy is ongoing as a normal process, abnormal autophagy can cause various neuromuscular degenerative diseases such as Alzheimer's disease, Parkinson's disease, and distal type myopathy.[1] In a specific type of cardiomyopathy (Danon disease), cardiomyocytes include marked autophagic vacuoles in the cytoplasm,[2] where dysfunction of the autophagic process is suggested by deficiency of the lysosomal protein Lamp-2.[3,4] Dilated cardiomyopathy (DCM) is a major cause of morbidity and mortality among congestive heart failure (CHF) patients and is associated with a continuous loss of cardiomyocytes.[5] At present, the mechanism of cardiomyocyte death in DCM is controversial, with apoptosis proposed by some researchers[6–8] but no apoptosis by others, including us.[9–11] Recent studies reported autophagic vacuoles in myocytes of heart diseases with failure such as DCM and aortic stenosis of the terminal stage,[11–14] but the pathophysiological significance in those diseases is still undetermined. Importantly, a basic issue such as the linkage between autophagic degeneration and cell death has not been evidenced in cardiomyocytes of failing hearts.

The UM-X7.1 hamster is an animal model of autosomal recessive cardiomyopathy and muscular dystrophy that is caused by lack of the δ-sarcoglycan gene and that develops a progressive cardiomyocyte death.[15,16] The

Supported in part by the Ministry of Education, Science, and Culture of Japan (research grants 15209027, 16590669, 16590721).

Accepted for publication October 18, 2005.

Address reprint requests to Hisayoshi Fujiwara, M.D., Ph.D., Second Department of Internal Medicine, Gifu University School of Medicine, 1-1 Yanagido, Gifu 501-1194, Japan. E-mail: gifuim-gif@umin.ac.jp.

condition begins at ~4 weeks of age and then worsens throughout subsequent weeks. Cardiac hypertrophy is seen by the time the animals are ~20 weeks of age and is followed by progressive ventricular remodeling and fibrosis with CHF. Approximately half of these animals die by the time they are 30 weeks old. Notably, one family and two sporadic cases of human DCM were recently identified in which the patients presented with mutations in the δ-sarcoglycan gene.[17]

It is widely accepted that granulocyte colony-stimulating factor (G-CSF), a regeneration- and/or repair-related cytokine, can alleviate postmyocardial infarction cardiac dysfunction and remodeling.[18–22] Recently, we reported that postinfarction treatment with G-CSF accelerated the healing process of myocardial infarction through augmenting macrophage accumulation in the infarcted area, up-regulating the matrix metalloproteinase (MMP) family, and inducing transdifferentiation of bone marrow cells into cardiomyocytes, although the incidence of transdifferentiation was small.[21] However, it is unknown whether the G-CSF treatment is effective against cardiac dysfunction due to nonischemic origin. Therefore, the aims of the present study were to define the mode of death of cardiomyocytes in UM-X7.1 hamster and to examine whether G-CSF exerts beneficial effects on the nonischemic failing hearts.

Materials and Methods

Animals

Male UM-X7.1 hamsters were provided by Drs. T. Ohkusa and M. Matsuzaki of Yamaguchi University School of Medicine, Ube, Japan. Male golden hamsters were chosen as the control without heart disease (Clea Japan, Shizuoka, Japan). The animals were housed in an air-conditioned room with an automatic 12:12 hours day-night cycle and maintained on a normal laboratory diet with free access to tap water. All animals received humane care in accordance with the Guide for the Care and Use of Laboratory Animals (NIH publication no. 8523, revised 1985).

Experimental Protocols

Protocol I: Examination of Autophagy

Male UM-X7.1 hamsters and the sex-matched golden hamster controls were sacrificed at the age of 30 weeks (n = 8 each).

Protocol II: Effect of G-CSF on Hamsters

Recombinant human G-CSF (Chugai Pharmaceutical Co., Tokyo, Japan) was administered at a dosage of 10 μg/kg/day to 16 male UM-X7.1 hamsters by subcutaneous injection on the first 5 days of each week. The injections were begun when the animals reached 15 weeks of age and were continued for 15 weeks, until the animals were 30 weeks of age. In the untreated group of UM-X7.1 hamsters, the same volume of distilled water (~50 μl per animal) was given to 15 age- and sex-matched hamsters throughout the same period. Age- and sex-matched golden hamsters were similarly treated with G-CSF (n = 8) or with distilled water (n = 6).

In another set of experiments, we examined the possibility of bone marrow-derived myocardial regeneration. Bone marrow cells were aspirated from the femoral bones of 12 UM-X7.1 hamsters at the age of 15 weeks and labeled by incubation for 30 minutes at 37°C with fluorescent carbocyanine 1,1′-dioctadecyl-1-3,3,3′,3′-tetramethyllindocarbocyanine perchlorate (DiI; Molecular Probes, Eugene, OR) as previously described.[23] Approximately 3×10^5 labeled mononuclear cells were then autologously returned to the bone marrow space of the femurs,[24] after which G-CSF or distilled water (n = 6 each) was administered to the animals as described above. Fifteen weeks later, hearts of hamsters assigned to this protocol were used exclusively to prepare cryosections.

Protocol III: In Vitro *Cell Death Assay*

Ventricular cardiomyocytes were isolated from 8-week-old male Sprague-Dawley rats and cultured overnight by the method previously described.[25,26] Culture media were replaced with glucose-depleted and 100 mmol/L mannitol-supplemented on the next day, as starvation is known to cause autophagic degeneration/death in various organs including the heart (glucose-starvation model).[27,28] G-CSF (0, 0.1, 1, 10, or 100 μg/L) was simultaneously added to the media, and the cardiomyocytes were cultured for 96 hours. Cell viability was assessed by cellular rod shape with trypan blue dye exclusion.[26]

Blood Sampling

Blood used for hemocounts was drawn from the retro-orbital sinus before treatment and from the inferior vena cava at sacrifice.

Assessment of Cardiac Function

Echocardiography and cardiac catheterization were performed before sacrifice as previously described.[29]

Tissue Processing and Histology

One day before sacrifice, Evans blue dye (1% v/v; Sigma, St. Louis, MO) was intraperitoneally injected to the randomly chosen animals (n = 3 from each group). This was to detect cardiomyocytes with increased membrane permeability.[29] The heart was transversely cut at the center between the atrioventricular groove and the apex. The basal half was fixed with 10% buffered formalin for histological examination. From the apical half, a small portion was removed and prepared as specimens for cryosections and for electron microscopy, and the rest was quickly immersed in liquid nitrogen for Western blotting

and zymographic analyses. Other main organs including lungs and livers were excised and histologically examined.

On preparations taken from the center of the ventricle and stained with Masson's trichrome, the percent fibrotic area (expressed by blue areas) was measured using a multipurpose color image processor LUZEX F (Nireco, Kyoto, Japan) by searching the entire ventricular slices. Cardiomyocyte size (as the transverse diameter of the cardiomyocyte cut at the nucleus level) was measured in the cells present in 20 randomly chosen high-power fields of the left ventricular free wall in each section. Numbers of cardiomyocytes, leukocytes, and macrophages were counted in a whole ventricular slice stained with hematoxylin and eosin.

In the animals injected with Evans blue dye 1 day before examination, the hearts were excised and cryosections were examined under a confocal microscope (LSM510; Zeiss, Jena, Germany) after nuclear staining with Hoechst 33342 (Sigma). The percentage of Evans blue-positive cells was calculated in 20 randomly chosen high-power fields in each section. We also examined Evans blue-positive cells without a nucleus to check whether those cells were actually dying.

Immunohistochemistry

The cardiac sections were incubated with a primary antibody against ubiquitin (DAKO Japan, Kyoto, Japan), cathepsin D (DAKO), Rab7 (Santa Cruz Biotechnology, Santa Cruz, CA),[30] von Willebrand factor (DAKO), phosphorylated Akt (p-Akt; Cell Signaling, Beverly, MA), or phosphorylated signal transducer and activator of transcription-3 (p-Stat3, Cell Signaling). An ABC kit (Vector Laboratories, Burlingame, CA) was used for the immunostaining of the deparaffinized sections with diaminobenzidine as the chromogen and nuclei were stained with hematoxylin. Positive control sections for autophagic degeneration were obtained from mouse liver after 24 hours of starvation.[27] For immunofluorescence, Alexa Fluor 488 (Molecular Probes) was the secondary antibody and nuclei were then stained with Hoechst 33342. After immunofluorescence the sections were observed under the confocal microscope.

In situ nick end-labeling assays were performed to detect apoptotic cells using an ApopTag kit (Chemicon Int., Temecula, CA) according to the manufacturer's instructions. Positive control sections were from mouse mammary gland. The percentage of immunopositive cells was calculated in 20 randomly chosen high-power fields in each section.

Using hearts from the animals receiving autologous implantation of the DiI-labeled bone marrow cells 15 weeks before, the ventricles were cut into three transverse blocks. At least 20 cryosections (6-μm thick) from each block, and thus more than 60 cryosections from each heart, were made. They were then immunostained using the primary antibody against troponin I (Chemicon), von Willebrand factor (DAKO), or α-smooth muscle actin (Sigma). In a preliminary study, we checked the pattern of DiI uptake by bone marrow cells and by cultured adult rat ventricular cardiomyocytes that were obtained by the method previously described.[25,26] For all sections, unanimous interpretation of the staining was acquired from two observers blinded to the specimen's group.

Electron Microscopy

Cardiac specimens or cultured cardiomyocytes were fixed with phosphate-buffered 2.5% glutaraldehyde (pH 7.4) and postfixed with 1% osmium tetroxide, after which they were conventionally processed for electron microscopy (H700; Hitachi, Tokyo, Japan). Terminal dUTP nick-end labeling (TUNEL) assay at the electron microscopic level (EM-TUNEL) was performed on ultrathin sections as previously described.[9]

Western Blotting

Proteins (100 μg) extracted from hearts were subjected to polyacrylamide gel electrophoresis and then transferred onto polyvinylidene difluoride membranes. The membranes were then probed using the antibody against ubiquitin, cathepsin D, Rab7, p-Akt, p-Stat3, phosphorylated extracellular signal-regulated kinase (p-ERK, Cell Signaling), or tumor necrosis factor-α (TNF-α; eBioscience, San Diego, CA), and the blots were visualized by means of enhanced chemiluminescence (Amersham Biosciences, Piscataway, NJ). The signals were quantified by densitometry. α-Tubulin (analyzed using antibody from Sigma) was a loading control.

Gelatin Zymography

The activity of MMP was measured using the gelatin-zymography kit (Yagai Research Center, Yamagata, Japan).

Statistical Analyses

Values are presented as means ± SEM. Analysis of survival was evaluated using the Kaplan-Meier method with the log-rank Cox-Mantel method. The significance of differences in the findings was evaluated using Student's *t*-test or one-way analysis of variance followed by the Newman-Keul's multiple comparison test. Values of $P < 0.05$ were considered significant.

Results

Cardiomyocyte Degeneration and Death in UM-X7.1 Hamsters

Spontaneous cardiomyocyte degeneration occurs in this strain.[15,16] Sarcolemmal integrity was assessed by living staining with Evans blue dye. The dye is excluded by cardiomyocytes with normal sarcolemmal permeability but taken up by cardiomyopathic cells with leaky cell

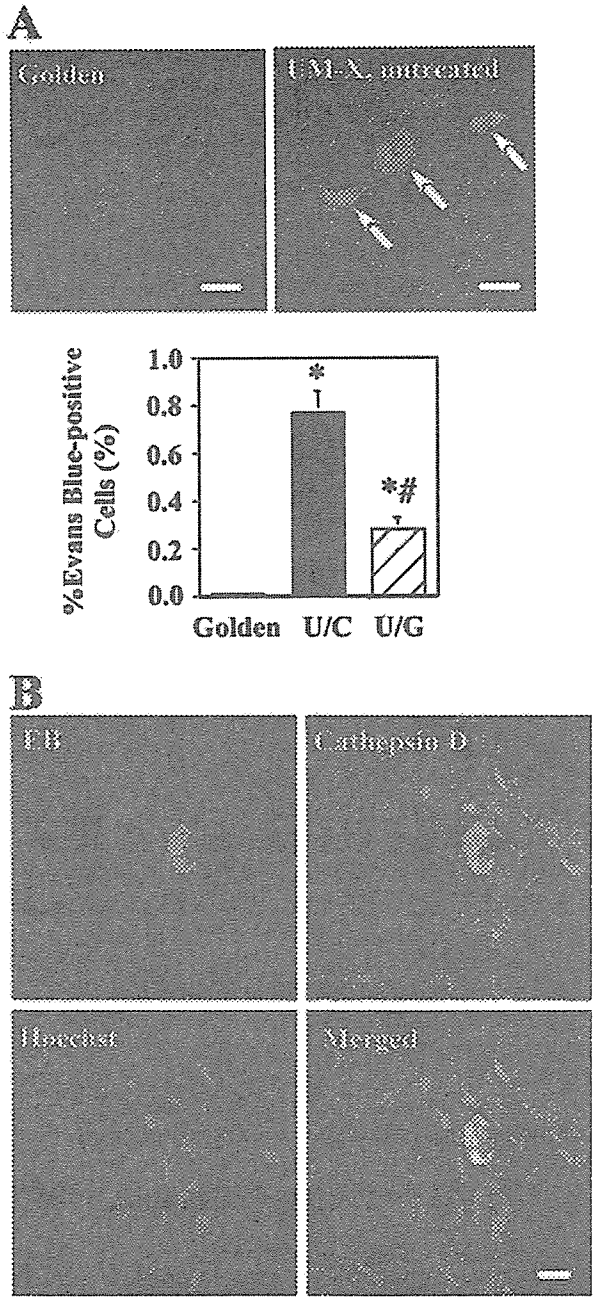

Figure 1. Confocal micrographs. **A:** Myocardium from the golden (**left**) and untreated UM-X7.1 (**right**) hamsters injected with Evans blue dye. Red fluorescence (**arrows**) indicates uptake of Evans blue; blue fluorescence shows nucleus. Percentages of cells taking up Evans blue are compared in the bar graph on the **right**. C, untreated golden hamster; C-U, untreated UM-X7.1 hamster; and U-G, G-CSF-treated UM-X hamster. $^{*}P < 0.05$. **B:** Myocardium from the untreated UM-X7.1 hamster injected with Evans blue (red) and immunostained for cathepsin D (green). Nuclei (blue) are counterstained with Hoechst 33342. Scale bars, 50 μm (**A**); 10 μm (**B**).

membranes.[29] No cardiomyocyte was found to include Evans blue in golden hamsters. However, the hearts of UM-X7.1 hamsters exhibited extensive dye uptake (Figure 1A). Nuclei were absent in 6.7 ± 0.7% of Evans blue-positive cardiomyocytes in the untreated UM-X7.1 hearts, implying ongoing death in those cells.

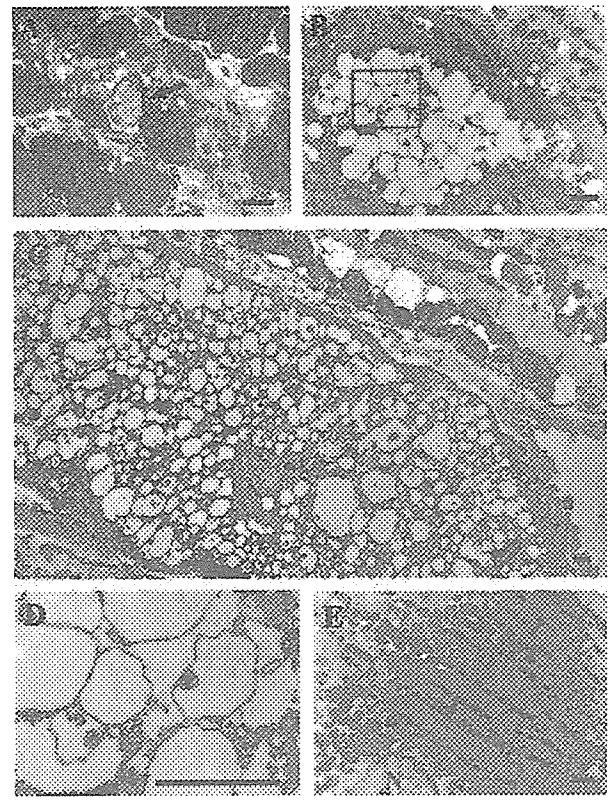

Figure 2. **A** to **D:** Light and electron micrographs showing severe vacuolar degeneration in cardiomyocytes from untreated UM-X7.1 hearts. **A:** A semithin section showing a cardiomyocyte with severe vacuolar degeneration (**arrow**). **B** and **D:** The vacuoles contained degraded subcellular organelles (eg, mitochondria) as indicated by **arrows** in **D** and thus appeared autophagic vacuoles. **C:** An example of a cardiomyocyte in which the cytoplasm is almost replaced by vacuoles. **Arrows** indicate barely remaining myofibrils. Such degenerative changes were attenuated in the G-CSF-treated group (**E**). Nucl, nucleus. Scale bars, 10 μm (**A**); 1 μm (**B–E**).

Ultrastructural analysis of the hearts revealed various grades of autophagic degenerative changes in cardiomyocytes (Figure 2, A–D). By contrast, we found no clear evidence of interstitial cell degeneration/death in the UM-X7.1 hearts. In addition, immunostaining for ubiquitin, cathepsin D, and Rab7 revealed significantly higher incidences of cardiomyocytes in the UM-X7.1 hamsters than in the hearts of golden hamsters (Figure 3, A–D). In particular, ubiquitin and cathepsin D were expressed as granular cytoplasmic inclusions (Figure 3, A and B). Western blotting confirmed up-regulation of ubiquitin, cathepsin D, and Rab7 in the hearts of UM-X7.1 hamsters (Figure 3, E and F). Next, to examine whether such degeneration may be causatively related with cell death, we observed the hearts of animals injected with Evans blue after immunostaining for cathepsin D. We found that almost all Evans blue-positive cardiomyocytes were also positive for cathepsin D (Figure 1B), suggesting a direct linkage between autophagic degeneration and death in cardiomyopathic cells.

Rare TUNEL-positive cardiomyocytes were found, although significantly more in UM-X7.1 hamsters than in golden hamsters (Figure 4A). EM-TUNEL revealed that TUNEL-positive cardiomyocytes exhibited not apoptotic

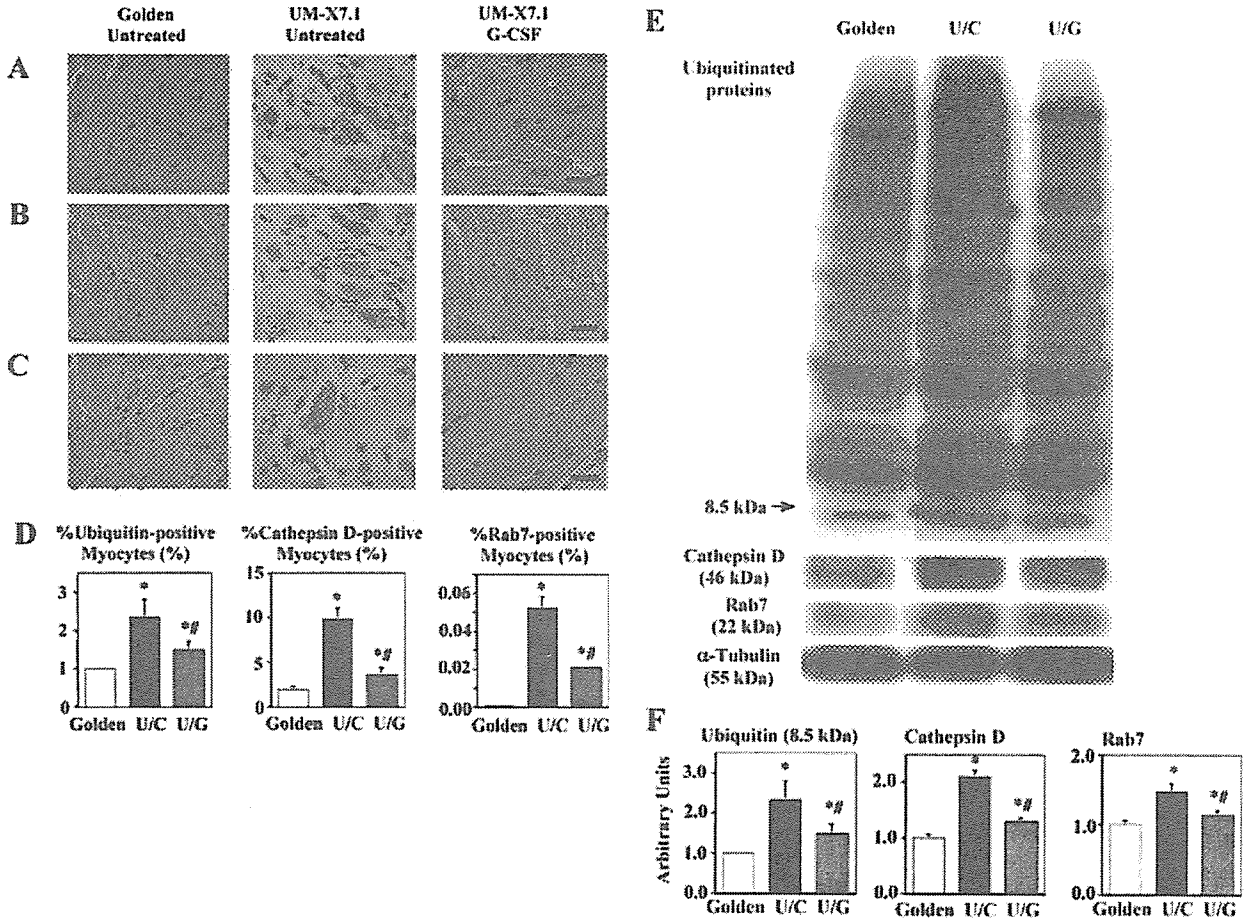

Figure 3. Immunohistochemistry and Western blotting for markers of autophagy. **A–C:** Immunostaining for ubiquitin (**A**), cathepsin D (**B**), and Rab7 (**C**) in the myocardium. **D:** Percentages of the immunopositive cells are compared in the bar graphs. **E** and **F:** Western blots for myocardial ubiquitin, cathepsin D, and Rab7 (**E**) and graphs showing densitometry (**F**). In ubiquitin blotting, the whole gel image is shown to demonstrate the distribution of ubiquitinated substrates. $P <$ 0.05 compared with the value of untreated golden hamsters (*) or that of untreated UM-X7.1 hamsters (#). Scale bars, 20 μm.

ultrastructure but hypertrophied nuclei (Figure 4B). This finding was consistent with human DCM, as previously reported,[9] and suggests a false-positive TUNEL reaction as apoptosis. Catalytic activity of both MMP-2 and MMP-9 in the heart was significantly higher in the UM-X7.1 hamsters compared with the golden hamsters (Figure 5A). Cardiac TNF-α levels were up-regulated in the 30-week-old UM-X7.1 hamsters (Figure 5B).

Effect of G-CSF to UM-X7.1 Hamsters

Hemocount

Granulocyte counts in animals treated with G-CSF for 15 weeks reached 14,921 ± 1037 cells/μl, which was significantly greater than the counts obtained from untreated controls (774 ± 65 cells/μl) or the baseline counts obtained from the groups before the treatment (694 ± 168 cells/μl). There was no significant difference in red blood cell or platelet counts between the groups.

Improvement of Survival and Cardiac Function and Structure

Although 7 of 15 untreated UM-X7.1 hamsters died by 30 weeks of age (survival rate, 53%), all 16 hamsters (100%) treated with G-CSF survived 30 weeks (Figure 6). All golden hamsters, with or without G-CSF-treatment, survived until the age of 30 weeks. At 30 weeks of age, all of the surviving animals underwent echocardiography and cardiac catheterization. The untreated UM-X7.1 hamsters showed severe left ventricular (LV) enlargement and signs of decreased cardiac function compared with the untreated golden hamsters (Figure 7): low LV ejection fraction (%EF), high LV end-diastolic pressure, and reduced ±dp/dt. All of those parameters were significantly improved in the G-CSF-treated animals (Figure 7). On the other hand, there was no difference in systolic LV pressure, diastolic aortic pressure, or heart rates between the untreated and G-CSF-treated UM-X7.1 hamsters. G-CSF did not affect cardiac function of golden hamsters (data not shown).

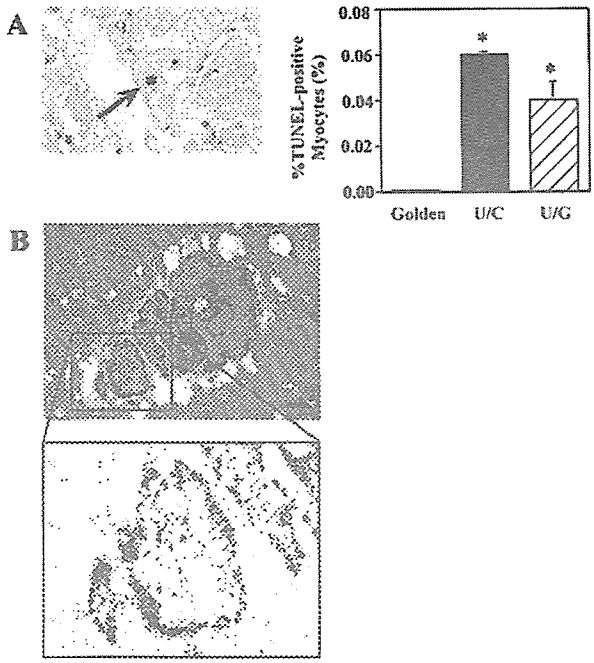

Figure 4. TUNEL and EM-TUNEL assays. **A:** Photograph of a TUNEL-positive cardiomyocyte (**arrow**) in the heart of untreated UM-X7.1 hamster and graph showing the percentage of TUNEL-positive cardiomyocytes among groups. $^*P < 0.05$ compared with untreated golden hamsters. **B:** An EM-TUNEL-positive cardiomyocyte reveals that such a cell is not ultrastructurally apoptotic, suggesting a false-positive TUNEL reaction as apoptosis.

The hearts of untreated UM-X7.1 were bigger and heavier at necropsy than those of golden hamsters, but the degree was attenuated in the G-CSF-treated UM-X7.1 (Figure 8, A and C). Histologically, there were numerous fibrotic foci and abundant interstitial fibrosis in the ventricles of untreated UM-X7.1 hearts, which were significantly mitigated in the ventricles of G-CSF-treated hearts: percent

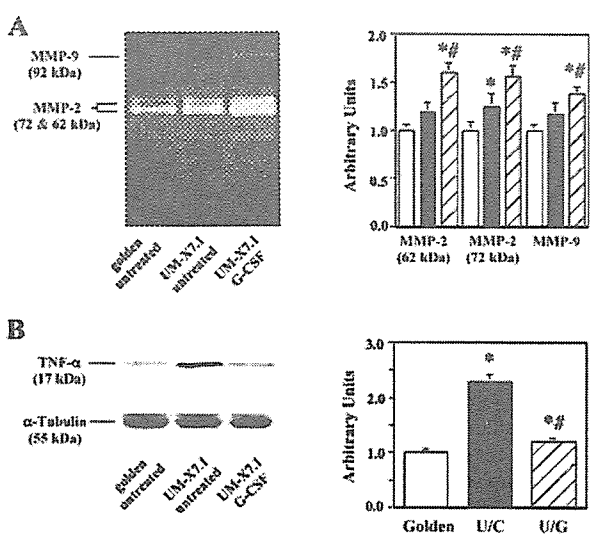

Figure 5. Effect of G-CSF on MMP catalytic activity and expression of TNF-α protein in hearts. **A:** Gelatin zymogram. **B:** Western blot for TNF-α. The bar graphs summarize the quantifications by densitometry. $P < 0.05$ compared with the value of untreated golden hamsters (*) or that of untreated UM-X7.1 hamsters (#).

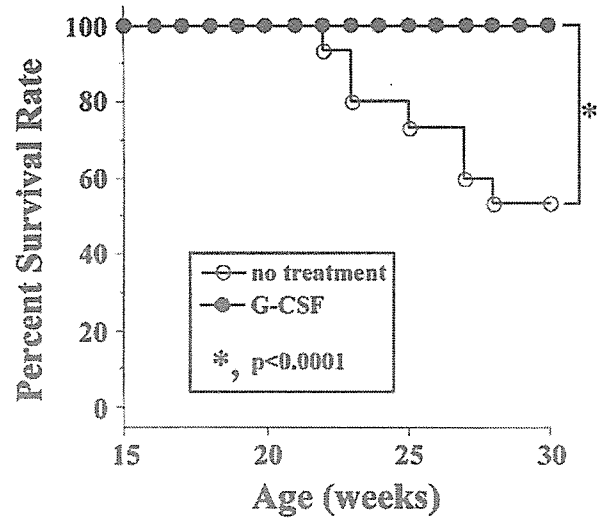

Figure 6. Effect of G-CSF on the survival curve for cardiomyopathic hamsters. The treatment was started at 15 weeks of age and continued until 30 weeks of age.

area of ventricular fibrosis was 20.2 ± 2.3% in the untreated group versus 8.6 ± 1.0% in the G-CSF group of UM-X7.1 hamsters (Figure 8, B and D). In fact the percent area of fibrosis in the G-CSF group at 30 weeks of age was not different from that seen before treatment, when the animals were only 15 weeks of age (7.3 ± 1.3%, $n = 6$). Cardiomyocyte population per ventricular slice was smaller in the untreated UM-X7.1 compared with that in golden hamsters, which was partially restored by the G-CSF treatment (Figure 8E). Such an attenuated fibrosis and restored cardiomyo-

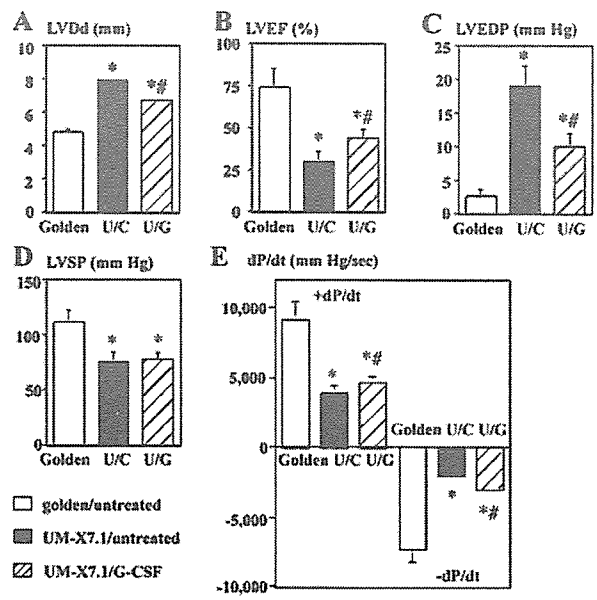

Figure 7. Effect of G-CSF on cardiac function based on echocardiography (**A** and **B**) and cardiac catheterization (**C–E**). C, untreated golden hamster; U/C, untreated UM-X7.1 hamster; U/G, G-CSF-treated UM-X7.1 hamster. LVDd, left ventricular end-diastolic diameter; LVEF, left ventricular ejection fraction; LVEDP, left ventricular end-diastolic pressure; LVSP, left ventricular peak systolic pressure. $P < 0.05$ compared with the value of untreated golden hamsters (*) or with that of untreated UM-X7.1 hamsters (#).

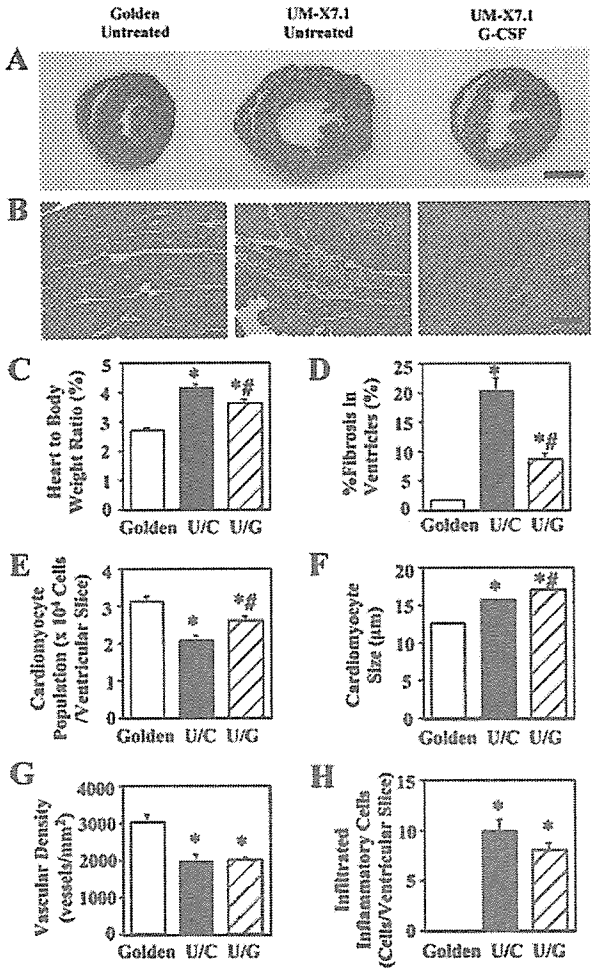

Figure 8. Effect of G-CSF on cardiac pathology. **A:** Light micrographs of the whole ventricular slices. Masson's trichrome stain. **B:** Highly magnified photographs of the myocardial tissue. **C–E:** Graphs showing the heart to body weight ratio, the percent areas of fibrosis in the ventricles, the numbers of cardiomyocytes in a whole ventricular slice, the size of cardiomyocytes, vascular density, and the infiltrated inflammatory cell population. $P < 0.05$ compared with the value of untreated golden hamsters (*) or with that of untreated UM-X7.1 hamsters (≠). Scale bars: 5 mm (**A**); 100 μm (**B**).

cyte population in hearts suggest a protective effect of G-CSF against cardiomyocyte dropout in the cardiomyopathic hamster. The cardiomyocyte size of the untreated UM-X7.1 hamsters was greater than that of golden hamsters, and the increase in the size was significantly augmented by the G-CSF treatment (golden, 12.6 ± 0.24 μm; untreated UM-X7.1, 15.7 ± 0.27 μm; and G-CSF-treated UM-X7.1, 17.0 ± 0.19 μm; $P < 0.05$) (Figure 8F). Vascular density in myocardium was significantly reduced in UM-X7.1 hamsters, compared with golden hamsters. Treatment with G-CSF did not affect the density in UM-X7.1 hamsters (Figure 6G). Inflammatory cell infiltration into the myocardium was rare in both groups of UM-X7.1, although greater compared with that in golden hamsters, and the numbers of infiltrated inflammatory cells (granulocytes, lymphocytes, and macrophages) were similar between the untreated and G-CSF-treated UM-X7.1 (Figure 8H). When we examined the animals for adverse reactions, including splenic rupture, splenomegaly, thromboembolism, interstitial pneumonia, and atherosclerosis, we detected no notable adverse effect of G-CSF.

Preventive Effect of G-CSF on Autophagic Alteration but Not on Incidence of TUNEL-Positive Cardiomyocytes

The incidence of cardiomyocytes with Evans blue dye uptake was clearly decreased in the G-CSF-treated hearts of UM-X7.1 hamsters, compared to that of the untreated group (Figure 1A). Cardiomyocytes with autophagic degenerative ultrastructure were diminished in the G-CSF-treated group (Figure 2E). In addition, immunostaining for ubiquitin, cathepsin D, and Rab7 revealed significantly lower incidences of cardiomyocytes in the G-CSF-treated hearts (Figure 3, A–D). Western blotting confirmed these findings (Figure 3, E and F). These suggest that G-CSF exerts a protective effect against autophagic degeneration and death of cardiomyocytes. The incidence of TUNEL-positive cardiomyocytes was similar between the untreated and G-CSF-treated UM-X7.1 hamsters (untreated, 0.06 ± 0.001% versus G-CSF, 0.04 ± 0.008%, P = n.s.) (Figure 4A).

Activation of Downstream Signals of G-CSF

The binding of G-CSF to its receptor evokes signal transduction through activation of Janus kinase (Jak)/Stat; Akt kinase, which has been identified as a downstream target of phosphatidylinositol-3′-kinase (PI3K); and mitogen-activated protein kinase (MAPK)/ERK.[21,31,32] Western blot analysis revealed that treatment with G-CSF resulted in a significant up-regulation of p-Stat3 and p-Akt, but not of p-ERK, in UM-X7.1 hearts (Figure 9, A and B).

Immunohistochemistry revealed that p-Stat3 distributed on cardiomyocytes whereas p-Akt was exclusively on endothelial cells in the G-CSF-treated UM-X7.1 hearts (Figure 9C). And, both proteins appeared more intensely expressed in the G-CSF-treated hearts compared with the untreated ones. This suggests that Jak/Stat pathway may contribute for cardiomyocyte protection, consistent with the previous report.[22]

Increase in MMP Catalytic Activity and Decrease in TNF-α Content in the Heart

The MMP catalytic activity was significantly increased in the G-CSF-treated group, compared to that of the untreated group (Figure 5A). G-CSF significantly reduced cardiac TNF-α levels (Figure 5B).

No DiI-Labeled (Bone Marrow-Derived) Cardiomyocytes and Vascular Cells

In another set of experiment, we evaluated the mobilization of DiI-labeled bone marrow cells into the heart. In our preliminary study, DiI was taken up by both bone marrow cells and cultured adult cardiomyocytes and was

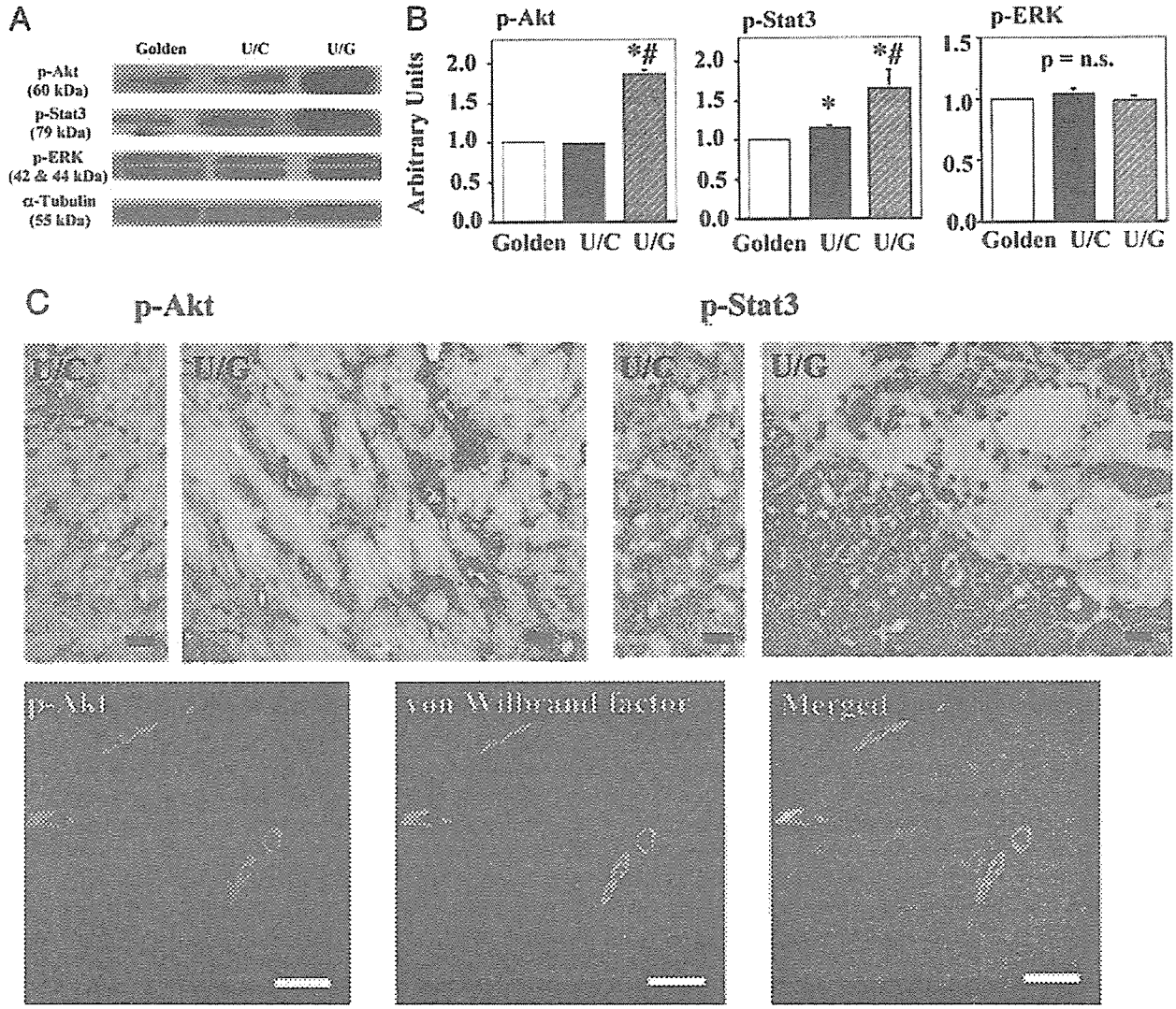

Figure 9. Downstream signals of G-CSF. **A** and **B:** Western blotting for myocardial p-Akt, p-Stat3, and p-ERK. The graphs show the densitometry (**B**). **C:** Immunohistochemistry for p-Akt and p-Stat3 in the untreated and G-CSF-treated UM-X7.1 hearts. P-Akt localized on endothelial cells whereas p-Stat3 localized on cardiomyocytes. Confocal images show p-Akt localization on von Willebrand factor-positive endothelial cells. Scale bars: 10 μm (**C, top**); 50 μm (**C, bottom**).

distributed in a spotty pattern (Figure 10A), similar to that seen previously in neuronal cells.[23] Extensive examination by confocal microscopy revealed no cardiac cells, ie, cardiomyocytes, endothelial cells, vascular smooth muscle cells, or interstitial cells, were positive for DiI in any hearts, in the G-CSF-treated and untreated hearts (Figure 10B).

Effect of G-CSF on Cultured Adult Cardiomyocytes

After 96 hours, survival rate was markedly reduced when cardiomyocytes were cultured in glucose-depleted media (Figure 11A). Electron microscopy confirmed many autophagic vacuoles in the cardiomyocytes with glucose starvation (Figure 11A). Addition of G-CSF significantly improved the survival in a dose-dependent manner (Figure 11B).

Discussion

Autophagy as the Major Mode of Cardiomyocyte Death in Nonischemic Cardiomyopathy

In the present study, we found abundant autophagic degeneration in cardiomyocytes of the cardiomyopathic hamsters, in which cathepsin D and Rab7 were overexpressed. Importantly, we suggested that cardiomyocyte death succeeds to autophagic degeneration based on the finding that most of the cardiomyocytes with disrupted plasma membrane were positive for cathepsin D. Although TUNEL-positive cardiomyocytes were more frequently found in the cardiomyopathic hamsters than in the healthy hamsters, the positivity rate was very low and moreover, the false-positive reaction of TUNEL as apo-

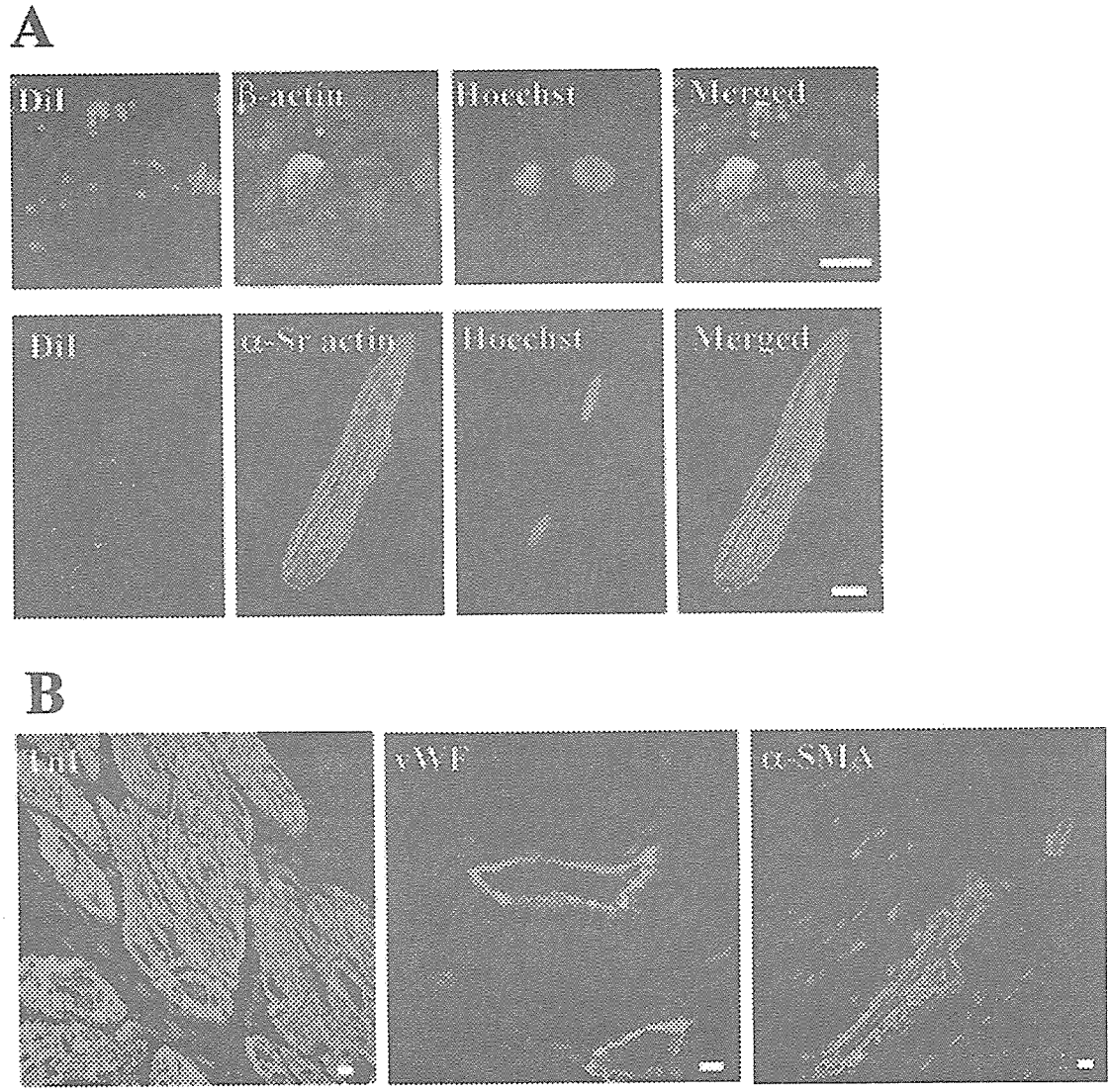

Figure 10. Confocal photomicrographs. **A:** Merged images of DiI fluorescence (red), immunostaining of the indicated cellular protein (green), and Hoechst 33342 (blue). **Top**: Smear of bone marrow cells showing DiI labeling and immunostaining of β-actin (green) using anti-β-actin antibody (Sigma). **Bottom**: Cultured rat cardiomyocytes labeled with DiI and α-sarcomeric actin (green) detected by anti-α-sarcomeric actin antibody (DAKO). These are positive control sections for DiI. **B:** Myocardium from a G-CSF-treated UM-X7.1hamster. No DiI spots (red) are observed, merging with green fluorescence of troponin I, von Willebrand factor, or α-smooth muscle actin. Nuclei (blue) are counterstained with Hoechst 33342. Scale bars, 10 μm.

ptosis was suggested by the EM-TUNEL assay. This is consistent with a recent report indicating apoptosis does not significantly contribute to cardiomyocyte dropout in another DCM hamster model (glycoprotein-sarcoglycan deficiency) similar to ours.[33] Thus, autophagy rather than apoptosis is the major mode of cardiomyocyte death of the present cardiomyopathic hamster.

TNF-α, which is elevated in patients with heart failure, is not only a cytotoxic cytokine that directly depresses cardiac function,[34] it also up-regulates angiotensin II type 1 receptor, thereby contributing to angiotensin II-mediated organ fibrosis.[35] In general, members of the MMP family are up-regulated in CHF, and in postmyocardial infarction models of CHF, their inhibition has a beneficial effect on cardiac remodeling and function.[36] It is believed that increases in MMP can exacerbate heart failure by catalyzing collagen degradation. In addition to autophagy of cardiomyocytes, the up-regulation of these cytokines may play an important role as pathogenesis of cardiac heart failure in this model.

Beneficial Effect of G-CSF on Cardiomyopathic Hamsters and the Mechanisms

G-CSF treatment improved survival, cardiac function, and fibrosis. It reduced autophagic degeneration of cardiomyocytes as indicated by ultrastructure and immunopositivity for cathepsin D and Rab7. Although it is known that G-CSF can induce transdifferentiation of stem cells in bone marrow into cardiac cells, we could not find DiI-labeled cardiomyocytes and vascular cells in hearts. Our